far as that is possible in the presence of the occupied state (lm)):

$$|\, l^3;\, v=1\ L=l\ M=m\ \sigma\rangle \sim a^+(lm\sigma)\sum_{m'} a^+(lm'\uparrow)a^+(l\bar{m}'\downarrow)\,|0\rangle \tag{4.13}$$

where the seniority quantum number $v = 1$ indicates that only a single nucleon is present in an unpaired orbit. (Note that in (4.13) we have included the specification of the spin coordinate of the individual nucleons, $\sigma = \uparrow$ or $\downarrow$ and have taken cognizance of the fact that the orbit corresponding to the time reversed $(lm\uparrow)$ is $(l\bar{m}\downarrow)$.) If a fourth particle is now added, it can be correlated with the odd particle in (4.13) in the same manner in which the first two particles were correlated, yielding the correlated four-particle (= two-pair) state

$$|\,(l^4)\ v=0\ I=0\rangle = \mathcal{N}_4\left(\sum a^+(lm\uparrow)a^+(l\bar{m}\downarrow)\right)^2|0\rangle$$

$$\mathcal{N}_4 = \left\{2^2(2l+1)2l\right\}^{-1/2} \tag{4.14}$$

Continuing in this manner, we generate the lowest configurations for an arbitrary number of particles in the so-called seniority coupling scheme [30]:

$$|\,(l^{2N})\ v=0\ I=0\rangle = \mathcal{N}_{2N}\left(\sum a^+(lm\uparrow)a^+(l\bar{m}\downarrow)\right)^N|0\rangle$$

$$\mathcal{N}_{2N} = \left\{(N!)^2\binom{2l+1}{N}\right\}^{-1/2} \tag{4.15}$$

where the last factor in the normalization is the binomial coefficient that counts the number of different N-pair basis states $a^+(\nu_1)a^+(\bar{\nu}_1)\cdots a^+(\nu_N)a^+(\bar{\nu}_N)$ that are linearly superposed in (4.15). It is an elementary exercise to verify that the expectation value of the interaction (4.5) acting in the state (4.15) is

$$\langle l^{2N}\ v=0\mid V_p\mid l^{2N}v=0\rangle = -G(\Omega-N+1)N \tag{4.16}$$

where

$$\Omega = 2l+1 = \#\text{ of pair states } (\nu\bar{\nu}) \text{ in the configuration considered} \tag{4.17}$$

For the ground states of the odd particle configurations, this calculation yields

$$\langle l^{2N+1}\ v=1\ L=l\mid V_p\mid l^{2n+1}\ v=1\ L=l\rangle = -G(\Omega-N)N \tag{4.18}$$

We see that the seniority coupling scheme implies:
(i) The binding of N pairs increases linearly with N as long as $N \ll \Omega$. This reflects the fact that each particle is correlated to a partner within its pair, but is uncorrelated with particles in other pairs (aside from the anti-correlation implied by the Fermi statistics). The effects of the anti-symmetry are small as long as N is small compared to Ω.

(ii) The odd particle configurations are displaced upward in energy with respect to the average of the neighboring even ground states by an energy

$$\Delta = -\frac{1}{2}\{E(2N, v=0) - 2E(2N+1, v=1) + E(2N+2, v=0)\}$$

$$= \frac{1}{2}G\Omega \tag{4.19}$$

This effect is a direct reflection of the fact that the odd particle does not participate in the correlation that is measured by the interaction (4.5).
(iii) The basic reaction that probes the correlations in the state (4.15) is pair addition, described by the matrix element

$$\langle N+1\ v=0\mid A^+\mid N\ v=0\rangle = \sqrt{(N+1)(\Omega-N)}$$

$$\text{where } A^+ = \sum_{\nu}^{\Omega} a^+(\nu)a^+(\bar{\nu}) \tag{4.20}$$

The factor $\sqrt{N+1}$ on the right-hand side of (4.20) reflects the fact that the $v = 0$ state is a "condensate" of N identical boson-like pairs.
The seniority coupling scheme provides us with a useful model that illustrates the nature of the many-body correlations associated with pairing, but the model system (4.6) is the one we want to study since, as we have already seen (in Table 3), the single-particle energies $\epsilon(\nu)$ play an important role in determining the pair-correlated state. Thus, the condensate should be built out of the more general pair-correlated state

$$A^+ = \sum c(\nu)a^+(\nu)a^+(\bar{\nu}) \tag{4.21}$$

rather than the state in which the amplitudes are ν-independent as in (4.15). The many-particle state vector created by $(A^+)^N$ is now considerably more complicated than that obtained in the degenerate approximation. This complication can be overcome with sufficient computing power, but a much more illuminating solution to this problem was discovered by Bardeen, Cooper, and Schriefer (1957) in the wave function that they proposed for the metallic super conducting state. They argued that the essence of the pairing interaction (4.5) is to distribute the particles as smoothly and broadly as possible over the available paired bases $(\nu\bar{\nu})$: this tendency is resisted by the one-particle energies $\epsilon(\nu)$, which favor configurations in which the lowest possible single-particle states are occupied. The most favorable occupation will thus be a compromise depending on the relative strengths of these two tendencies. This way of looking at the problem suggest that the effect of the

pairing interaction may be described by a mean field obtained by linearizing (4.5):

$$-G\left(\sum a^+(\nu)a^+(\bar{\nu})\right)\left(\sum a(\bar{\nu})a(\nu)\right)$$
$$\rightarrow -GM\left[\sum(a^+(\nu)a^+(\bar{\nu})+a(\bar{\nu})a(\nu)\right]$$
$$M=\frac{1}{2}\left\langle\sum(a^+(\nu)a^+(\bar{\nu})+a(\bar{\nu})a(\nu))\right\rangle \tag{4.22}$$

The mean field in (4.22) is seen to be an operator that creates and destroys pairs of particles with a constant amplitude in all the available paired orbits $(\nu\bar{\nu})$. The average, M, that determines the strength of the pair field is taken in the ground state of the Hamiltonian that includes the linearized interaction (4.22). The ground state of this linearized problem can be written as a product of factors describing the degree of occupation of each of the paired states:

$$\Psi_{BCS}=\Pi_\nu(U_\nu+V_\nu a^+(\nu)a^+(\bar{\nu}))\,|\,0\rangle \tag{4.23}$$

The coefficients (U_ν, V_ν) are to be chosen so as to minimize the energy in the state (4.23) and in order to ensure normalization, we set

$$U_\nu^2+V_\nu^2=1 \tag{4.24}$$

The close connection between the BCS state and the pair condensate considered above can be seen by introducing a gauge angle, $(e^{i\Theta})$, in the state (4.23)

$$\Psi_\Theta=\Pi(U_\nu+e^{i\Theta}V_\nu a_\nu^+ a_{\bar{\nu}}^+)\,|\,0\rangle \tag{4.25}$$

and expanding in powers of this phase

$$\Psi_\Theta=(\Pi U_\nu)\left\{1+e^{i\Theta}\sum\frac{U_\nu}{V_\nu}a_\nu^+a_{\bar{\nu}}^++e^{2i\Theta}\left(\sum\frac{V_\nu}{U_\nu}a_\nu^+a_{\bar{\nu}}^+\right)^2+\cdots\right\} \tag{4.26}$$

Thus, if we integrate Ψ_Θ weighted by $e^{-iN\Theta}$, we recover a pair condensate wave function in the form discussed above:

$$\int_o^\pi e^{-iN\Theta}\,\Psi_\Theta\,d\Theta\sim\left(\sum c(\nu)a_\nu^+a_{\bar{\nu}}^+\right)^N\,|\,0\rangle$$
$$c(\nu)=\frac{V(\nu)}{U(\nu)} \tag{4.27}$$

The integration over Θ is seen to be a projection operator projecting onto the state with N-pairs. The occurrence of a mean field that causes fluctuations in particle number has a certain novelty and so it may be useful to explore some of the features involved in using the state vector (4.23):

Problem 1.

Show that

$$\langle N\rangle=\left\langle\frac{1}{2}\sum a^+(\nu)a(\nu)+a^+(\bar{\nu})a(\bar{\nu})\right\rangle=\sum_{\nu=1}^{\Omega}V_\nu^2$$
$$\langle N^2\rangle=\langle N\rangle^2+\sum U_\nu^2V_\nu^2 \tag{4.28}$$

thus, for the degenerate case, we have

$$V(\nu)=\sqrt{\frac{N}{\Omega}}\qquad U(\nu)=\sqrt{1-\frac{N}{\Omega}}$$
$$\sigma^2=\langle N^2\rangle-\langle N\rangle^2=N\left(1-\frac{N}{\Omega}\right)\ll N^2 \tag{4.29}$$

Problem 2.

Because of the particle number fluctuations, it is necessary to add a term depending linearly on the particle number in order to constrain the solution so that, at least on the average, the particle number has the correct value. Thus, the linearized Hamiltonian becomes

$$H'=\sum\epsilon(\nu)(a^+(\nu)a^+(\nu)+a^+(\bar{\nu}))$$
$$-GM(\sum a^+(\nu)a^+(\bar{\nu})+a(\bar{\nu})a(\nu))$$
$$-\lambda\sum(a^+(\nu)a(\nu)+a^+(\bar{\nu})a(\bar{\nu}) \tag{4.30}$$

Show that on taking the expectation value of H' in the state (4.23), and minimizing the energy with respect to (U_ν, V_ν) subject to (4.24) and choosing λ so that

$$\frac{1}{2}\left\langle\sum a^+(\nu)a(\nu)+a^+(\bar{\nu})a(\bar{\nu})\right\rangle=N \tag{4.31}$$

one obtains

$$U_\nu^2=\frac{1}{2}\left[1+\frac{\epsilon(\nu)-\lambda}{\sqrt{(\epsilon(\nu)-\lambda)^2+\Delta^2}}\right]$$
$$V_\nu^2=\frac{1}{2}\left[1-\frac{\epsilon(\nu)-\lambda}{\sqrt{(\epsilon(\nu)-\lambda)^2+\Delta^2}}\right] \tag{4.32}$$

where Δ and λ are obtained by solving the two equations

$$\sum V_\nu^2 = \frac{1}{2}\sum_\nu \left(1 - \frac{\epsilon - \lambda}{\sqrt{(\epsilon-\lambda)^2 + \Delta^2}}\right) = N$$

$$\frac{G}{2}\sum \frac{1}{\sqrt{(\epsilon(\nu)-\lambda)^2 + \Delta^2}} = 1 \tag{4.33}$$

The further analysis of spectra built on a ground state with the structure (4.23) is a very beautiful chapter in many-body theory which, however, is beyond the scope of the present chapters. I shall therefore complete the present chapter with a discussion of experimental measurements of nuclear properties that test this description and provide quantitative values for the parameters that are involved:

(a) The odd–even effect in nuclear binding:
From the earliest studies of nuclear binding energies, it was recognized that the binding of odd A nuclei is systematically somewhat weaker than that of nuclei in which the number of neutrons and of protons are both even numbers [31]. A quantitative measure of the odd–even binding effect for neutrons is provided by the parameter

$$\Delta_n(N, Z) = \frac{1}{4}\{\mathcal{B}(N-2, Z) - 3\mathcal{B}(N-1, Z) + 3\mathcal{B}(N, Z) - \mathcal{B}(N+1, Z)\} \tag{4.34}$$

where $\mathcal{B}(N, Z)$ is the binding energy of the nucleus with N neutrons and Z protons. For protons, the odd–even energy difference is obtained by interchanging N and Z in (4.34). The values of Δ_n and Δ_p obtained in this manner are plotted in Fig. 27; it is seen that there are considerable fluctuations (reflecting local variations in the level densities and in the strength of the effective pairing interaction), but on the average the data follow approximately the value

$$\Delta \approx \frac{12\ \text{MeV}}{A^{1/2}} \tag{4.35}$$

This dependence reveals, first of all, that the pairing energy is a correlation effect since the simple twofold Kramer degeneracy of orbits in the mean field would only produce an odd–even effect of the order A^{-1}. But, at the same time, the $A^{1/2}$ dependence seen in (4.35) implies that the effect extrapolates to $\Delta = 0$ in nuclear matter ($A = \infty$), i.e. the observed pairing must be interpreted as a surface effect reflecting the stronger effective attraction of nucleons in the lower density surface region. (Surface pairing might have been expected to imply an $A^{-1/3}$ dependence for Δ, and indeed, more recent analyses of odd–even energy differences which take account of the dependence of Δ on the neutron excess parameter $(N-Z/A)^2$ indicate that the dependence of the leading term in Δ should be $A^{-1/3}$ [32].

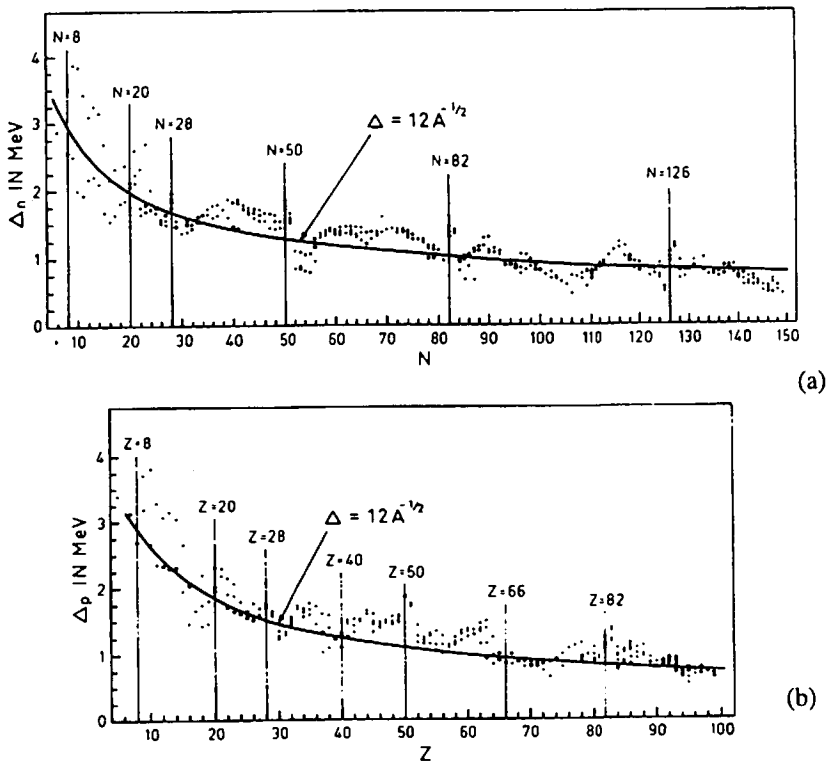

Fig. 27. Systematics of odd–even mass difference. The quantity $\Delta_n(N)$ is obtained from the measured binding energies by means of Eq. (4.34).

From the value (4.33), we can obtain an independent estimate of the pairing coupling constant G to compare it with (4.8). Solving equations (4.33) for a constant level density, d, extending over an interval $(-\frac{1}{2}S, +\frac{1}{2}S)$ around the chemical potential λ, we obtain

$$\Delta = S \exp\left\{-\frac{d}{G}\right\} \tag{4.36}$$

Keeping the same set of neutron orbits as in the discussion of ^{206}Pb, we have

$$S \approx 4\ \text{MeV} \qquad d \approx \frac{4\ \text{MeV}}{22} = 0.18\ \text{MeV} \tag{4.36a}$$

which implies

$$G = 0.12 \quad \text{for} \quad A \approx 200. \tag{4.36b}$$

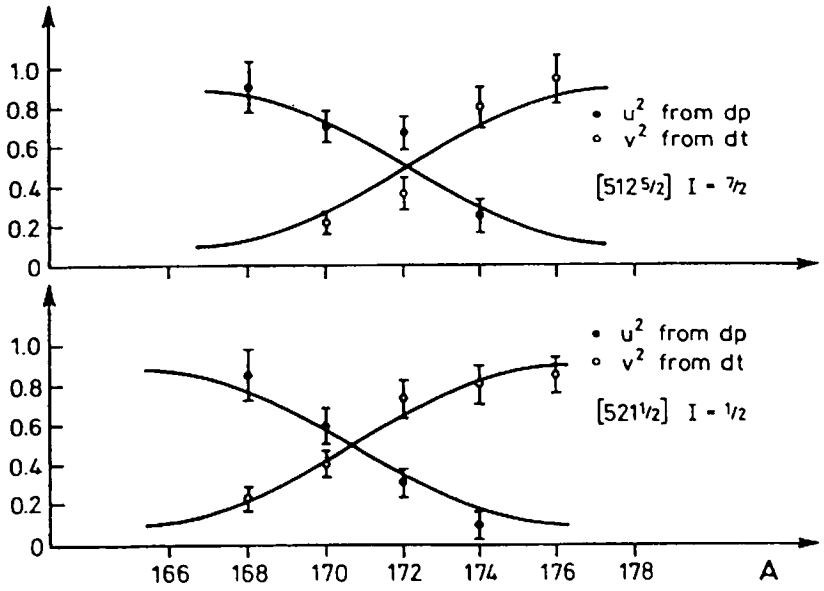

Fig. 28. Occupation probabilities for single-particle states in Yb isotopes as a function of the number of neutrons, N.

(b) The expressions (4.32) describe the smooth transition from occupied to unoccupied states at the Fermi surface implied by the configuration mixing that underlies the pair correlations. These occupation probabilities can be measured in one-particle transfer reactions and, in particular, in a series of measurements that compare the occupancies of the same single-particle orbit in a sequence of nuclei with different particle numbers. Such data, shown in Fig. 28, establish the rate of variation of the chemical potential as compared with the ratio Δ/d; i.e. occupancy of an orbit as a function of neutron orbit N is

$$V^2(N) = \frac{1}{2}\left\{1 + \frac{N - N_o}{\sqrt{(N - N_o)^2 + \gamma^2}}\right\} \tag{4.37a}$$

$$\gamma = \Delta\left(\frac{d\lambda}{dN}\right)^{-1} = \frac{2\Delta}{d} \tag{4.37b}$$

where N_o is the neutron number for which the orbit is half occupied. From Fig. 28, we obtain

$$\gamma = 3.2 \tag{4.38a}$$

which, together with the level spacing appropriate for these mid-shell deformed nuclei ($d \approx 0.35$ MeV), yields

$$\Delta \approx 0.6 \text{ MeV} \tag{4.38b}$$

which can be compared with the value $\Delta_n = 0.7$ MeV obtained from the odd–even differences in binding energies in this region (see Fig. 27).

(c) The one-particle transfer cross sections measure the square of the occupation amplitudes, but the correlation in the pair condensate depends on the coherence in phase of all the admixed amplitudes; this coherence is reflected in the enhancement of the cross sections for two-particle transfer going from ground state to ground state of the pair-correlated system. Thus, calculating the pair addition amplitude in the state (4.23):

$$\langle \psi_{BCS} \mid \sum a^+(\nu)a^+(\bar{\nu}) \mid \psi_{BCS} \rangle = \sum U_\nu V_\nu = \frac{\Delta}{G} \tag{4.39}$$

where in the last line we have used (4.32) and (4.33). The cross section for adding a correlated pair of neutrons as in the (tp) reaction is proportional to the square of the matrix element (4.39). Experimental data illustrating this enhancement are shown in Fig. 29 in this example, the odd–even mass differences imply $\Delta_n = 1.4$ MeV, while $G \approx 0.2$ MeV (from (4.8) and (4.35) and assuming that G scales as A^{-1}), which implies an expected enhancement of the ground state transition in Fig. 29 by a factor $(\Delta/G)^2 \approx 50$.

(d) A final major effect resulting from the pair correlation concerns the moment of inertia for the low-lying rotational states in deformed nuclei. This topic might have been included in a later chapter in connection with the analysis of rotational motion, but since the detailed calculation of moments of inertia lies beyond the scope of these chapters, at this point it seems appropriate to summarize the main facts and the qualitative features that connect the observed phenomena with the pair correlations.

If the nucleons in a rotating nucleus responded as independent particles moving in the rotating mean field, the moment of inertia describing the rotational energy would have on the average the value corresponding to the rotation of a rigid body with the same density distribution as the nucleus (the derivation of this result employs a semi-classical approximation (Fermi–Thomas) and otherwise follows exactly Niels Bohr's argument [33] for the vanishing of orbital diamagnetism in a classical plasma (see, e.g., [25], p. 79).

The observed moments of inertia for low-lying rotational states are about a factor of two smaller than the rigid-body value. This reduction in the moment of inertia is attributed to the effect of the pair correlations. Indeed, if the pair

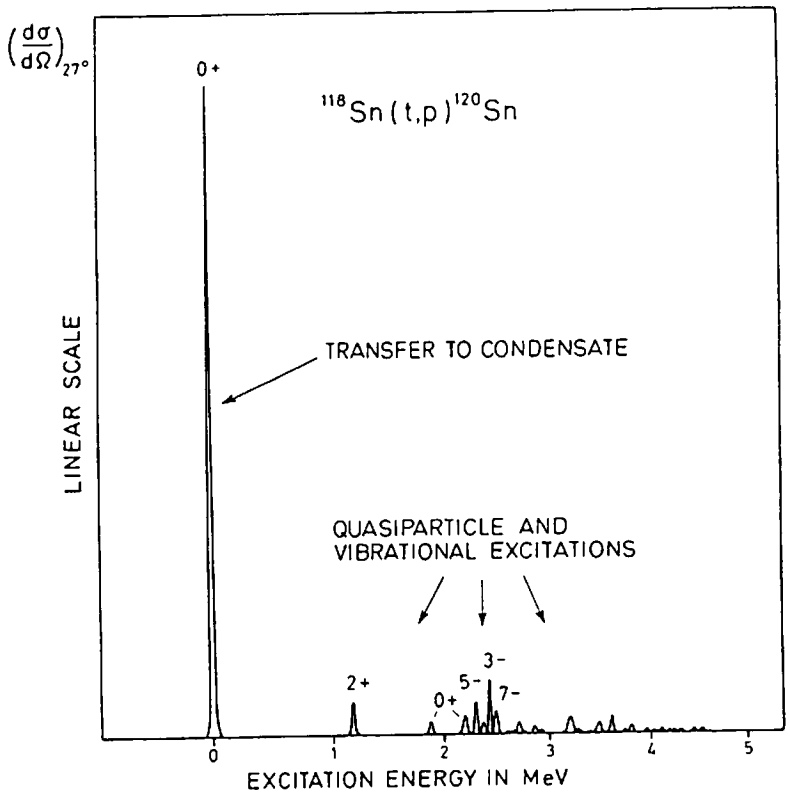

Fig. 29. Observed cross cross-section for two-particle transfer reaction. The enhancement of the ground state to ground state reaction reflects the existence of a condensate of $J = 0$ pairs in the ground state wave function.

correlations were very strong, the nucleus would respond to rotation as a Bose liquid, which for slow rotation responds with a collective velocity distribution derived from potential flow (irrotational) which gives rise to a moment of inertia that is smaller than the rigid-body value by a factor proportional to the square of the deformation, $(\Delta R/R)^2$. The size of the observed pairing in nuclei is not sufficiently strong to achieve this limit, as can be seen from the coherence length, ξ, that measures the size of the pairs in an infinite medium:

$$\xi = \frac{\hbar v_F}{\Delta}$$

where v_F is the Fermi velocity. Using the value (4.35) and $v_F = 1.0 \times 10^{10}$ cm/sec, the resulting coherence length ($\xi = 5.3A^{1/2}$ fm) is several times greater

than the nuclear radius, telling us that the pairs will not be able to respond as localized bosons, as is indeed revealed by the fact that the observed moments of inertia are much greater than the irrotational value described above. A detailed calculation of the moments of inertia based on the ground state wave function (4.23) is able to account for the observed value that lies intermediate between the rigid and irrotational values (see [25], p. 82 ff).

5. Deformation and rotation

In addition to pairing, there is a second mechanism based on geometrical deformation of the mean field, which particles in partially filled shells can exploit in order to build correlations that lower the energy. The tendency to generate such deformations can be traced back to the fact that the individual-particle orbits in a degenerate configuration are highly anisotropic. Thus, we shall begin by reviewing some of the features associated with the shapes of single-particle orbits.

As already discussed in Chapter 4, a single particle with angular momentum l and $m = l$ is associated with a density distribution that is pancake-like, concentrated in the $x - y$ plane with an angular thickness $\sim l^{-1/2}$. The states with $m \ll l$ have densities that are concentrated in the neighborhood of the z-axis.

In situations where there are approximate degeneracies in the single particle states, there may occur a superposition of states with different angular momentum (hybridization) and such states can exhibit especially interesting shapes. Thus, the shapes of organic molecules are strongly effected by the near degeneracy of the s and p electronic orbits in the carbon atom; these four orbits can be combined in several different ways to produce molecular orbits appropriate to different bonding geometries. For example the sp^3 combinations:

$$\begin{aligned}
\psi_1 &= \tfrac{1}{2}\left\{Y_{00} + \sqrt{3}\,Y_{10}\right\} \\
\psi_2 &= \tfrac{1}{6}\left\{3Y_{00} - \sqrt{3}\,Y_{10} + 2\sqrt{3}\,(Y_{11} + Y_{1-1})\right\} \\
\psi_3 &= \tfrac{1}{6}\left\{3Y_{00} - \sqrt{3}\,Y_{10} + \sqrt{3}\left(-1 + i\sqrt{3}\right) Y_{11} + \sqrt{3}\left(-1 - i\sqrt{3}\right) Y_{1-1}\right\} \\
\psi_4 &= \tfrac{1}{6}\left\{3Y_{00} - \sqrt{3}\,Y_{10} + \sqrt{3}\left(-1 - i\sqrt{3}\right) Y_{11} + \sqrt{3}\left(-1 + i\sqrt{3}\right) Y_{1-1}\right\}
\end{aligned} \tag{5.1}$$

represent directed bonds with electrons pointing in the four directions that define the vertices of a tetrahedron. Such deformed states provide the starting point for the development of the molecular orbital description of a tetrahedrally coordinated carbon atom, as in CH_4.

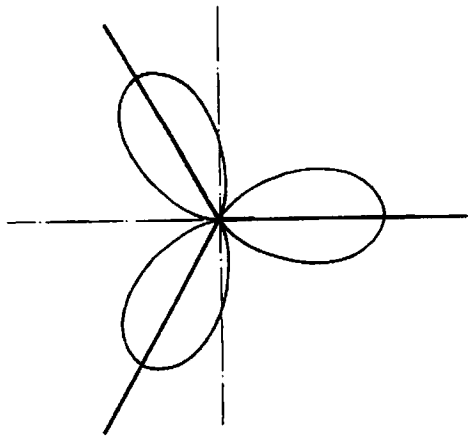

Fig. 30. Density distribution for hybridized orbits with $\Delta l = 3$. The figure plots the angular distribution of density in the equatorial plane for the function (5.2).

Another example of significant shapes of one-particle orbits results from the approximate degeneracies of states with angular momentum l_0 and l_0+3 that occur for the classical triangular orbits in a spherical potential that were discussed in the third chapter; these states can be hybridized in the combinations

$$\psi_1 = \frac{1}{\sqrt{2}}\left(Y_{l_0 l_0} + Y_{l_0+3, l_0+3}\right)$$

$$\psi_2 = \frac{1}{\sqrt{2}}\left(Y_{l_0 \bar{l}_0} + Y_{l_0+3, \overline{l_0+3}}\right) \tag{5.2}$$

which both have densities concentrated in the $x - y$ plane, and in this plane have densities that point in the directions of the three corners of an equilateral triangle (Fig. 30).

There are, of course, many other interesting shapes that can be generated by linear combinations of degenerate single-particle states, but the basic idea remains the same as illustrated in these examples. The occurrence of degeneracies in the single-particle spectrum is associated with the existence of a symmetry group for the single-particle hamiltonian, and the degenerate set of orbits provide a basis for a multi-dimensional irreducible representation of this symmetry; thus, of necessity any single one of these orbits will be a state which is *not* invariant under the full symmetry of the group, and therefore can be associated with a spontaneous breaking of the original symmetry.

We are now almost ready to take up the discussion of deformations, but first I want to make one more preliminary comment: the pairing effects that were discussed in the last chapter are a very different type of correlation from that associated with deformation. Indeed, the isotropy of the $J = 0$ pairs implies that the latent anisotropy of the degenerate one particle orbitals is suppressed to the extent that the pairing force is able to determine the nuclear coupling scheme. We shall later return to the issue of the competition between deformation and pairing, but begin by discussing deformations in the absence of pair correlations.

There are many different ways in which to express the fact that anisotropies in the shape of single-particle orbits will imply a tendency to collective deformations of the nucleus. We shall discuss a number of these different formulations, since these different pictures help to strengthen our understanding and imaginative use of the concepts.

1. The occurrence of angular anisotropy in the single-particle wave functions implies that a particle occupying such a state will exert an anisotropic pressure on the nuclear surface. For a closed shell, the simultaneous occupation of all the $2j + 1$ different orientations of the orbit with angular momentum j implies that the total pressure on the surface is isotropic, but for a partially filled shell there will in general be an anisotropic pressure and the total energy of the state will then be lowered by a collective deformation of the whole system.

2. The mean field that determines the orbits of the individual nucleons is generated by the nucleons themselves and, since the range of the nuclear forces is small compared with the nuclear radius, there is a strong tendency for the potential to have, as far as possible, the same shape as the density distribution. Thus, anisotropy in the density implies anisotropy in the potential.

3. A single particle in an orbit $(j, m = j)$ will give rise to a component in the mean field which is attractive for particles moving in the equatorial plane. The different m-states (j, m) are therefore no longer degenerate, but rather ordered so that those with the largest values of $|m|$ are lowest in energy. Thus, the next particle to be added to the nucleus will find its lowest energy by occupancy of the state $(j, m = -j)$. This will further enhance the strength of the mean field attracting particles into the equatorial plane. The third and fourth particles will go into $(j, m = j - 1)$ and $(j, m = -j + 1)$ and still further increase the anisotropy of the potential attracting particles to the equatorial plane. This "aligned" coupling scheme is seen to build on the fact that attractive interactions give rise to a feedback mechanism whereby the existence of an anisotropy in the mean field potential generates an ordering of the single-particle orbits so that the addition of subsequent particles tends, as far as possible, to further enhance the anisotropy. In this way, the particles in the partially filled shell achieve a maximum overlap that effectively exploits the attractive interactions between the particles.

4. The Jahn–Teller effect: The breaking of spherical symmetry for configurations involving partially filled shells in nuclei is an exact analogue of the lowering of the point symmetry of molecules in configurations where there is degeneracy

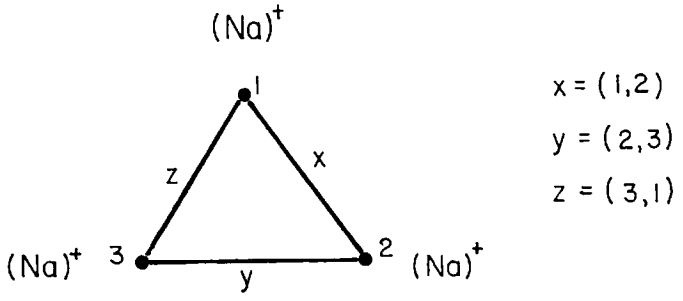

Fig. 31. Coordinates for describing a triangular molecule.

in the molecular orbitals of the electrons (see, for example, Landau and Lifshitz [34]). We shall illustrate this effect with a simple example, the details of which can be worked out as a homework exercise. We consider a schematic version of the triatomic molecule Na_3 and treat the valence electrons in a tight binding approximation. In the absence of the valence electrons, the Na^+-ions are assumed to have an equilibrium configuration corresponding to an equilateral triangle with bond lengths, s. Thus, the Hamiltonian is (see Fig. 31 for notation)

$$H = \tfrac{1}{2}K\left\{(x-s)^2+(y-s)^2+(z-s)^2\right\} - t\,(x)\left(c_1^+c_2 + c_2^+c_1\right) - t\,(y)\left(c_2^+c_3 + c_3^+c_2\right) - t\,(z)\left(c_3^+c_1 + c_1^+c_3\right) \tag{5.3}$$

The second line of Eq. (5.3) describes the hopping of the electrons from one ion to the next. The hopping matrix elements, t, depend on the bond lengths x, y or z and can be expanded for lengths near the equilibrium value

$$t(x) = t_o - \alpha(x-s) \tag{5.4}$$

For the ions in the position $x = y = z = s$, the electronic spectrum is as in Fig. 32. The ground state for the molecular cation, Na_3^+, is obtained by putting two electrons in the A orbital; this state is orbitally non-degenerate and the electrons are equally distributed on the three Na^+-ions preserving the symmetry of the equilateral triangle. The ground states for the neutral molecule Na_3 or the anion Na_3^- involve one or two electrons in the orbitally degenerate E-orbits; in these orbits, the electrons are not equally distributed on the three bonds and thus give rise to anisotropic stresses on the bond lengths. In particular, it can be seen that for an electron in the (E,α) state the hopping energy decreases linearly with increasing length of the x-bond. Thus, the equilibrium shape for the neutral molecule Na_3 is expected to be an obtuse isosceles triangle, as is indeed observed [35]. This example is a particular case of the general principle that a symmetric shape for the

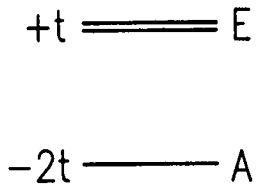

Fig. 32. Electronic spectrum for single electron moving in equilateral triatomic molecule. The eigen spectrum of the hamiltonian (5.3) is plotted for the symmetric case $t(x) = t(y) = t(z) = t$. The lowest state labeled, A is non-degenerate and has the wave function $\psi_A = \frac{1}{\sqrt{3}}(|1\rangle + |2\rangle + |3\rangle)$ while the two-fold degenerate excited state is described by the wave functions $\psi_{E_\alpha} = \frac{1}{\sqrt{2}}(|1\rangle - |2\rangle)$ and $\psi_{E_\beta} = \frac{1}{\sqrt{6}}(|1\rangle + |2\rangle - 2|3\rangle)$.

atoms in a molecule will in general be stable only for non-degenerate electronic states.

The basic geometrical facts responsible for the Jahn–Teller effect and nuclear deformations are identical as stated above, but the manifestation of the effect is somewhat different since in molecules the symmetry that is broken is that of a discrete point group, while in nuclei it is the three-dimensional rotation group; thus, the degeneracies in molecules are only of order unity, while in nuclei they are of order $A^{1/2}$.

The above discussion establishes the basic mechanism that tends to generate non-spherical shapes for the lowest configurations with many particles in unfilled shells. We now take up the questions, what shapes? and how much deformation? The shapes that will be selected are those that can be made to best fit the density distributions generated by the available single-particle orbits. The appropriate tool for studying these problems is the Nilsson diagram, which plots the energy of the single-particle states as a function of the parameters that describe the anisotropy of the potential in which these states are defined. We begin by illustrating this concept for an axially symmetric quadrupole potential acting in the space of single-particle states associated with a sharp value of the single-particle angular momentum, j,

$$V_{\text{def}} = -\beta V_0 Y_{20}(\theta) \tag{5.5}$$

$$\langle jm'|\,V_{\text{def}}|\,jm\rangle = -\beta V_0\sqrt{\frac{5}{4\pi}}\,\delta(m,m')\,(j\,1/2\;20\,|\,j\,1/2)\,(jm\,20\,|\,jm) \tag{5.6a}$$

$$= \beta V_0\sqrt{\frac{5}{4\pi}}\,\frac{3m^2 - j(j+1)}{j(j+1)} \tag{5.6b}$$

where V_0 is an average value of the spherical mean field and the parameter, β, measures the magnitude of the deformation; positive (negative) β corresponds

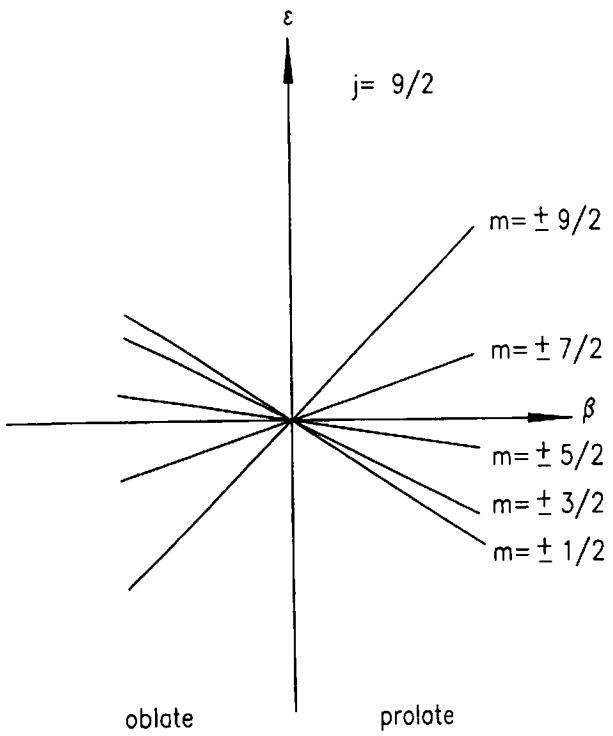

Fig. 33. Nilsson diagram for quadrupole deformation acting on a single particle with fixed total angular momentum, j.

to prolate (oblate) deformation. The last two factors in (5.6a) are vector addition coefficients that occur in the evaluation of the matrix elements of Y_{20} in the states $|jm\rangle$. The Nilsson diagram corresponding to the spectrum (5.6b) is drawn in Fig. 33. As discussed in connection with arguments for the aligned coupling scheme, the "natural" shape for a particle in an orbit with fixed angular momentum, j, is an oblate density lying in the plane perpendicular to the direction of the angular momentum; Fig. 33 exhibits this feature in the fact that the lowest energies are associated with the orbits $m = \pm j$ and oblate deformation. The energy is also lowered for $m = \pm 1/2$ and prolate deformation, but the energy gain for the latter choice is only half as much as that for the former, and so deformations at the beginning of a shell with a single value of j are expected to be oblate.

A single value of j is not an appropriate description of the shell structure encountered in heavy nuclei. A somewhat more appropriate picture is provided by

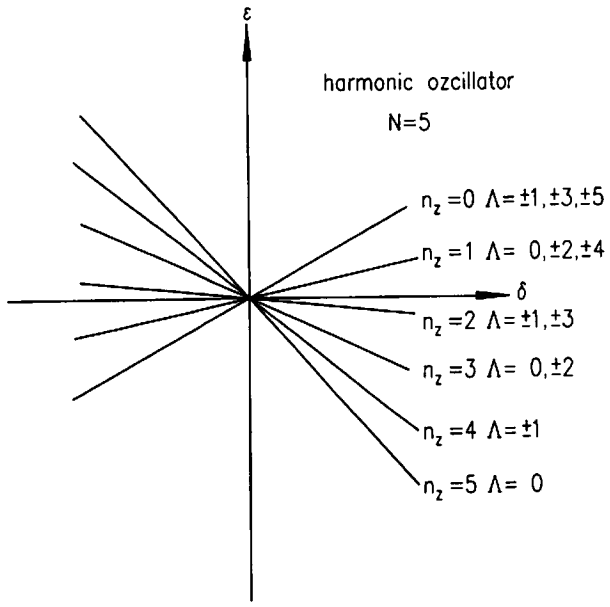

Fig. 34. Nilsson diagram for $N = 5$ shell of harmonic oscillator. The deformation is assumed to have axial symmetry with the symmetry axis in the z-direction. The orbits are labeled by n_z, the number of oscillator quanta in the z-direction and Λ, the component of orbital angular momentum along the z axis.

the major shells of the harmonic oscillator potential. If we consider an axially symmetric deformation of the spherical oscillator, the spectrum is given by

$$\epsilon\left(n_x n_y n_z\right) = \left(n_x + n_y + 1\right)\hbar\omega_\perp + \left(n_z + \frac{1}{2}\right)\hbar\omega_z \tag{5.7}$$

where the quantum numbers, n_κ, describe the number of oscillator quanta in each of the three spatial directions and the frequencies ω_z and $\omega_\perp$ characterize the strength of the restoring potential acting in the axial and perpendicular directions. The deformation parameter, δ, for such a deformed oscillator can be defined as

$$\delta = \frac{\omega_\perp - \omega_z}{\overline{\omega}}$$

$$\overline{\omega} = \tfrac{1}{3}\left(2\omega_\perp + \omega_z\right) \tag{5.8}$$

and the Nilsson diagram associated with a single major shell of the oscillator is drawn in Fig. 34. It is seen from this figure that the most favored orbits for a few

particles in such a shell will occur for prolate deformations and correspond to quantum numbers $(n_x n_y n_z) = (N, 0, 0)$, $(N-1, 1, 0)$, $(N-1, 0, 1)$, ...

The simple features illustrated in Figs. 33 and 34 quickly become considerably more complicated when we consider the shell structures actually encountered in heavy nuclei, see, for example, Fig. 35. Although this rich structure is fascinating and crucial for the specialists who are trying to understand the quantitative validity and consequences of these ideas, they lie outside the scope of a general course such as this, and I shall not attempt to explore these matters further except for a few general comments:

1. The connection between shell structure and periodic classical orbits provides very important guidance in considering what shapes are likely to be important. As discussed at the end of Chapter 3, the greatest number of degeneracies in the nuclear shell structure are associated with the classical orbits with $\omega_r : \omega_\phi = 2 : 1$ as for orbits in a spherical harmonic oscillator, or more generally for the pendulating orbits in any spherical potential. Such orbits have axial symmetry and give rise to deformations with even parity; the dominant effect is thus expected to be the spheroidal deformations described by (5.5), as is indeed observed.

2. The above discussion would suggest that there should be almost as many nuclei with prolate as with oblate shape, since for any prolate configuration of particles in a partially filled shell, there is a corresponding configuration of holes with respect to the filled shell for which the deformation is exactly equal but with opposite sign, i.e. oblate. This symmetry follows from the fact that the closed shell configuration yields a unique state in which the density distribution is isotropic. The observed deformations of nuclei are in dramatic disagreement with this expectation, being almost exclusively prolate. Detailed estimates of nuclear shapes based on the Nilsson diagram have been quite successful in interpreting the observed deformations, including the preference for prolate shapes. However, it is not yet understood whether this preference is the result of a general principle or whether it is a special feature of the nuclei that are available or that have been studied so far.

3. The connection between periodic orbits, shell structure and deformation suggests, as is indeed observed, that with increasing particle number the triangular orbits with $\omega_r : \omega_\phi = 3 : 1$ become increasingly important; the fact that an equilateral triangle has both quadrupole ($\lambda = 2$) and octupole ($\lambda = 3$) anisotropy implies that the latter deformations should become important, perhaps dominant if we consider shells with very large quantum numbers. Indeed, a few nuclei exhibiting static octupole shapes have been observed (see for example, the review by Butler and Nazarewicz [36]), and preliminary theoretical studies have confirmed that these shapes can be related to the $\Delta l = 3$ degeneracies that result from the triangular orbits. However, the space of deformation parameters becomes so large when all the $\lambda = 2$ and $\lambda = 3$ shapes are considered that it has not yet been possible to discover the general principles that determine the shapes resulting from the competition between all these different possibilities in a many-body configuration (see Hamamoto et al. [37] for a preliminary study of equilibrium shapes of configurations encountered while filling degenerate l_0 and $l_0 + 3$ orbits).

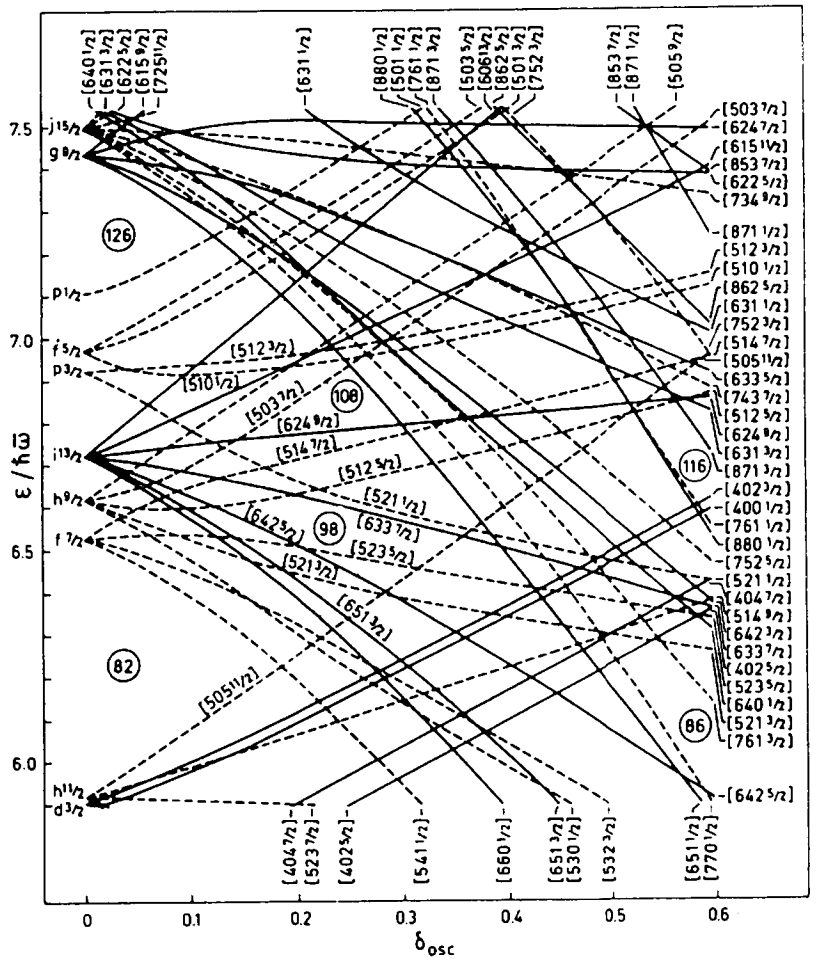

Fig. 35. Nilsson diagram for neutron orbitals in the $82 \leq N \leq 126$ shell. For $\delta = 0$, the spherical shell gaps and the spectroscopic labels are indicated. The orbits for non-zero deformation are labeled by quantum numbers $Nn_z\Lambda\Omega$ that are appropriate in the limit of an anisotropic spheroidal oscillator. The figure is taken from [25, p. 223].

4. The magnitude of the deformations that occur can be seen as a balance between the particles in the unfilled shells which move in intrinsically anisotropic orbits and the remaining (majority of) particles which occupy closed shells and therefore prefer the spherical shape. The order of magnitude of the resulting balance can be estimated by recognizing that the spherical shell structure results from a bunching together of the single-particle orbits that comprise the shell. The excess level density of single-particle orbits implies a stress (in the space of shapes) that is relaxed by the deformations. Thus, the magnitude of the equilibrium deformation (for a configuration in mid-shell) is determined by the condition that the spreading out of the single-particle levels in the Nilsson diagram implied by the deformation should be of the order of the energy spacing between shells. Thus, we obtain:

$$\text{spacing between shells} = \hbar\omega_{sh} \sim \frac{\hbar v_F}{L} \sim \epsilon_F / A^{1/3}$$

$$L = \text{length of classical orbit} \tag{5.9}$$

and since the dependence of the single-particle eigenvalues on deformation is,

$$\frac{d\epsilon}{d\beta} \sim \epsilon_F \tag{5.10}$$

we obtain in the estimate

$$\beta \sim A^{-1/3}. \tag{5.11}$$

That the slope of the single-particle orbits with deformation is of the order (5.10) can be verified in the examples (5.6) and (5.7) considered above. As can be seen from the representative values given in Table 4, the experimentally observed values of the nuclear deformations are in reasonable agreement with the qualitative estimate (5.11). Thus, the deformations in the low-lying states are small (as compared with unity), representing angular-dependent displacements of the nuclear surface through a distance of the order of the Fermi wave length. Such deformations are, however, sufficient to completely reorganize the single-particle orbits within a single major shell as revealed in the Nilsson diagram and, as we shall see below, lead to major effects in the low-energy spectra. (The so-called "super deformations" (see Chapter 7) are not small, and result from an aspect of shell structure different from that discussed above; the super deformations do not occur in the low-energy spectra except for the lightest nuclei.)

5.1. *Connection of deformation and rotation*

The existence of collective rotational excitations is deeply and inescapably connected with the occurrence of deformations in the density distribution of finite

Table 4

Systematics of nuclear deformations and rotational moments of inertia

Nucleus	E(2) (MeV)	$\tau_{1/2}$ (s)	$\mathcal{J}/\mathcal{J}_{rig}$	β	$\beta \times A^{1/3}$
^{24}Mg	1.37	1.35 (−12)	0.68	0.53	1.5
^{98}Sr	0.144	2.8 (−9)	0.65	0.40	1.8
^{164}Dy	0.073	2.4 (−9)	0.56	0.33	1.8
^{240}Pu	0.043	1.64 (−10)	0.52	0.24	1.5

The examples given in the table all represent nuclei near the middle of their respective shells and for which the rotational nature of the lowest excited states has been well established. The energy of the first excited, $I\pi = 2+$, state and it half-life, $\tau_{1/2}$, are given in columns two and three, respectively. In the latter datum, the number in parenthesis represents the appropriate power of 10. The rotational moment of inertia, $\mathcal{J}$, obtained from the energy $E(2)$ is given in column four: these moments are given in units of the moment for rigid rotation, which includes a correction for the axially symmetric deformation listed in column five. These deformations are derived from the measured lifetimes and energies of the $E2$ quadrupole transitions.

many-body systems. The necessity of these excitations can be recognized in the fact that the axes of the deformation can be chosen to point in any direction in space and all these different orientations are degenerate because of the rotational invariance of the underlying interactions that define the system. Thus, for a system exhibiting deformation it must be possible to (approximately) separate the many-body wave function into an intrinsic part $\chi_{int}(q)$ describing the motion of the particles with respect to a coordinate system oriented with respect to the deformation and a rotational part $D_{rot}(\theta)$ that describes the motion of the collective orientation with respect to the fixed laboratory coordinate system:

$$\psi = \chi_{int}(q)\, D_{rot}(\theta) \tag{5.12}$$

In order for this approximation to be useful, it is necessary to satisfy two conditions:

(a) the fluctuations in the deformation associated with the intrinsic motion must not be so large as to undermine the orientation of the deformation;

(b) the frequencies of the intrinsic motion that correspond to fluctuations in the deformation must be rapid compared with the frequency of rotational motion so that the former can be effectively averaged over in defining the rotational dynamics.

A closer examination of these two conditions reveals that they are in fact equivalent, as can be illustrated by analyzing the simple example of a diatomic molecule (see Fig. 36). The Hamiltonian describing the intrinsic vibration of the molecule is

$$H = \frac{1}{2}M\dot{R}^2 + \frac{1}{2}C(R - R_0)^2 \tag{5.13}$$

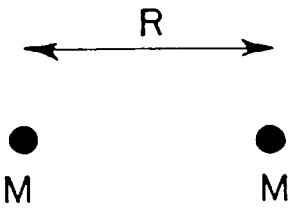

Fig. 36. Coordinates for a diatomic molecule.

which yields the vibrational frequency

$$\omega_{vib} = \sqrt{\frac{C}{M}} \tag{5.14}$$

and zero-point vibrational amplitude

$$(\Delta R)_{zero\ point} = \sqrt[4]{\frac{\hbar^2}{MC}} \tag{5.15}$$

Thus, the above condition (a) on the amplitude of the fluctuation in the deformation translates into

$$\frac{\Delta R}{R_0} = \sqrt[4]{\hbar^2/MCR_0^4} \ll 1 \tag{5.16}$$

while condition (b) on the frequency of intrinsic and rotational motion involves

$$\omega_{rot} = \frac{1}{\hbar}\frac{d}{dI}E_{rot} = \frac{d}{\hbar dI}\left(\frac{\hbar^2 I^2}{2MR_0^2}\right) = \frac{\hbar I}{MR_0^2}$$

$$\frac{\omega_{vib}}{\omega_{rot}} = \sqrt{\frac{C}{M}}\frac{MR_0^2}{\hbar} = \sqrt{\frac{MCR_0^4}{\hbar^2}} \gg 1 \tag{5.17}$$

When the above conditions (a) and (b) are satisfied, the separation (5.12) of rotational and intrinsic motion will be a good approximation and we expect

(a) for each intrinsic state χ, there will be a sequence of states (rotational band) resulting from the different possible superpositions of the degenerate orientations described by different functions D_{rot};

(b) the values of the total angular momentum, I, appearing in the sequence are determined by the symmetries of the deformed shape;

(c_1) the electromagnetic transitions between the different members of a rotational band provide a direct measure of the magnitude of the collective deformation since each such matrix element involves the expectation value of an electromagnetic moment in the intrinsic state χ responsible for the band;

(c_2) the relative values of the transition moments for different transitions within the band are purely geometric numbers representing the matrix elements of the different D-functions.

The full elaboration of these properties and their experimental verification goes beyond the scope of the present chapters, but I shall attempt in the following comments to illustrate some of the most important features:

1. The intrinsic excitations that set the limit on the accuracy with which the orientation can be defined are those generated by the Coriolis force, which is proportional to the single-particle rotation operator j_x (where the collective rotation is assumed to take place around the intrinsic x-axis). As can be seen from the examples treated in Figs. 33 and 34, the frequency of such excitations is of the order

$$(\hbar\omega)_{fluctuation} \sim \beta\hbar\omega_{sh} \sim \epsilon_F A^{-2/3} \tag{5.18}$$

Since the rotational frequencies are

$$\hbar\omega_{rot} \sim \frac{\hbar^2 I}{\mathcal{J}} \tag{5.19}$$

where $\mathcal{J}$ is the moment of inertia for rotation, the condition for separation between intrinsic and rotational motion becomes

$$\frac{\omega_{rot}}{\omega_{fluct.}} \sim \frac{\hbar^2 I}{\mathcal{J}} \cdot \frac{A^{2/3}}{\epsilon_F} \ll 1 \tag{5.20}$$

As discussed at the end of the previous chapter, the rotational moments of inertia would be equal to those of a rigidly rotating body if the nucleons responded to the inertial forces as independent particles, which implies

$$\frac{\hbar^2}{\mathcal{J}} \sim \frac{\epsilon_F}{A^{5/3}} \tag{5.21}$$

The observed nuclear moments of inertia are of order (5.21) though numerically somewhat smaller, as a result of the pair correlations (see Table 4). Employing (5.21) in (5.20), we find

$$I \ll A \tag{5.22}$$

as the limitation on the nuclear rotational angular momentum set by the zero-point fluctuations in the deformation.

2. The above arguments for the occurrence of rotational band structure in the spectrum of a nucleus exhibiting deformation can be recognized as repeating, almost word for word, the arguments for the occurrence of Goldstone bosons in the spectrum of a field theory in which the vacuum state violates a continuous symmetry of the Lagrangian or Hamiltonian. (The collective modes resulting from appropriately phased superpositions of the many different degenerate vacuum states.) In the many-body literature, however, you will discover that there is

almost universal agreement that "strictly speaking" such modes can only occur for infinite systems. However, since all physical systems are finite, it seems more appropriate to observe that there can hardly be any qualitative difference between a system with 10^{24} particles and one with 10^{20}, or 10^{14}, or 10^{6}, or 10^{4}, or .... The only differences that can be important for the smaller systems are associated with the possibility that fluctuations may limit the accuracy with which the order parameters (deformations) can be defined. Thus, in the latter systems it is important that the fluctuations and their effects be estimated as in the above discussion. But when the result of such an analysis is as in (5.22), the role of the Goldstone boson would seem to be just as inevitable and fundamental in the finite many-body systems as in the field theory models.

3. The overwhelming majority of deformed nuclei have shapes that preserve the following symmetries:

(i) axial symmetry;

(ii) invariance under rotation by 180° about an axis perpendicular to the symmetry axis, $\mathcal{R}_2(\pi)$;

(iii) invariance under:

space inversion, $\mathcal{P}$;

time reversal $\mathcal{J}$.

The reasons for the survival of these symmetries are, of course, a part of the analysis of the connection of shell structure and equilibrium shape that was briefly referred to above. In the presence of these residual symmetries of the intrinsic shape, the collective rotational degrees of freedom are correspondingly restricted.

Axial symmetry implies that for each single-particle state i, the component of angular momentum along the symmetry axis Ω_i, is a constant of the motion. In addition, there cannot be any collective rotation around this axis since there is no way in which a collective orientation could be defined in this dimension. Thus, the component K, of the total angular momentum with respect to this axis is determined by the sum of the single-particle contributions, Ω_i, and we have,

$$K = \Omega = \sum_i \Omega_i \tag{5.23}$$

The $\mathcal{R}_2$ symmetry implies that for each single-particle state Ω_i, there will be a degenerate single-particle state, i', with $\Omega_{i'} = -\Omega_i$ and thus the lowest configuration in an even– even nucleus has

$$K = \Omega = 0$$

$$\Psi = \chi_0 D^I_{M0}(\theta) \tag{5.24}$$

In addition, the $\mathcal{R}_2$ symmetry implies a reduction in the number of states in a rotational band, since it is not possible to distinguish the two orientations of the

symmetry axis that are related to each other by the $\mathcal{R}_2$ rotation; this restraint can be imposed by requiring that the effect of $\mathcal{R}_2^{(int)}$ acting on the intrinsic coordinates of χ_Ω should have the same effect on the total wave function as $\mathcal{R}_2^{(ext)}$ acting on the collective orientation angles θ appearing in D^I. Since

$$\mathcal{R}_2^{(int)} \chi_0 = \chi_0 \tag{5.25}$$

for the lowest configuration of even–even nuclei described above, while

$$\mathcal{R}_2^{ext} D^I_{MO} = (-1)^I D^I_{MO} \tag{5.26}$$

quite generally for the rotational D-functions with $K = 0$, we have for the ground state rotational bonds of even–even nuclei

$$I = 0,\ 2,\ 4,\ 6,\ \ldots \tag{5.27}$$

Fig. 37 shows examples of experimentally observed rotational bonds of even–even nuclei.

I shall not attempt to develop further the detailed connections between symmetries of the intrinsic states and the quantum numbers that characterize the associated rotational bonds, but the above example can serve to illustrate the detailed analogy with the manner in which the invariance properties of the broken symmetry ground state determine the quantum numbers of the Goldstone bosons.

4. The structure of matrix elements within a rotational band, referred to in point (c), above can be illustrated by the evaluation of the quadrupole matrix elements in the rotational band (5.24):

$$\left\langle I'K = 0 \,\|\, \sum_p r_p^2\, Y_2(p) \,\|\, IK = 0 \right\rangle = \sqrt{2I+1}\,\langle I0,\ 20 \mid I'0\rangle \left\langle \chi_0 \mid \sum_{p=1}^{A} r_p'^2\, Y_{20}(\theta_p') \mid \chi_0 \right\rangle \tag{5.28}$$

where the I-dependent factor is the vector addition coefficient that results from the evaluation of the integral over orientation angles

$$\int D^{I'}_{,0}\, D^2_{00}\, D^I_{,0}\, d\theta \tag{5.29}$$

while the last factor in (5.28) corresponds to the quadrupole moment of the intrinsic wave function χ_0. The measurement of such a matrix element provides a determination of the nuclear deformation, and the comparison of several different matrix elements within a single rotational bond tests the accuracy of the simple product wave function (5.24). Table 4 contains examples of measured values of nuclear intrinsic quadrupole moments obtained from E2 matrix elements within rotational bands, and of the deformation parameters derived from these moments.

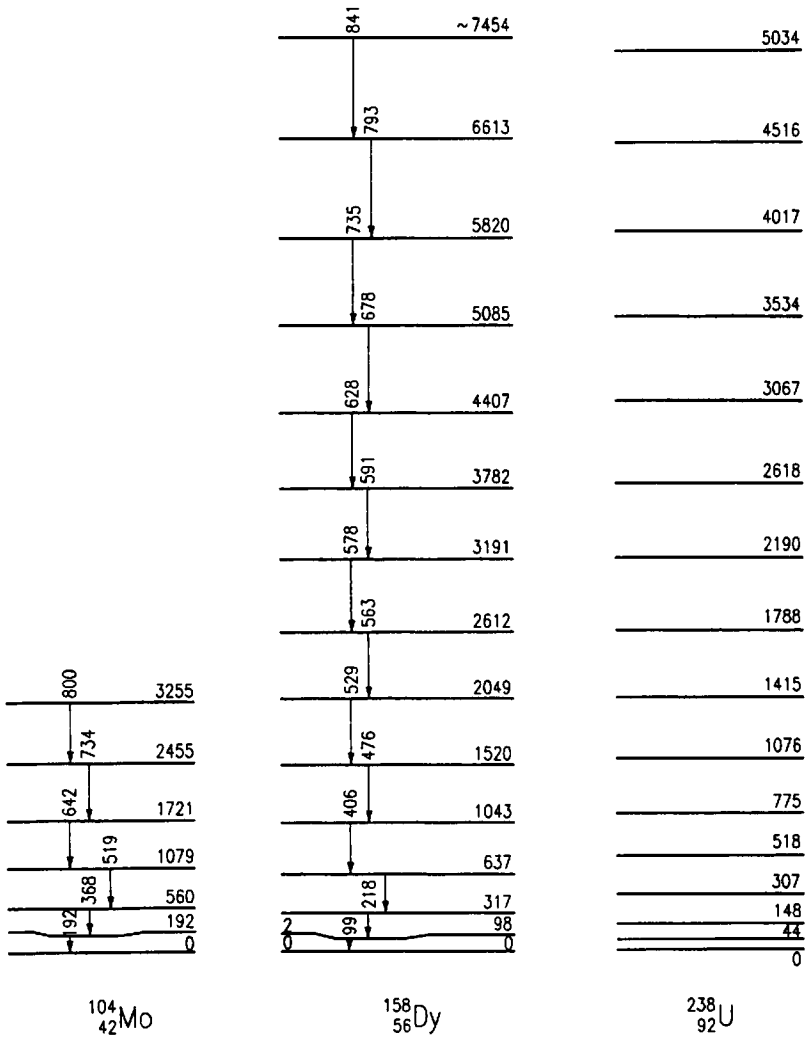

Fig. 37. Ground state rotational bands in ^{104}Mo, ^{158}Dy and ^{238}U.

6. Competition between pairing and deformation

We have so far considered pairing and deformation as simply two different possible types of correlation in configurations involving many particles outside closed

shells. In fact, both forms of correlation are simultaneously present in most spectra and can be seen as in unceasing competition with each other. The qualitative patterns in this competition can be understood from a discussion of the manner in which the correlations depend on the number of particles in the unfilled shells. For a configuration with just two particles in addition to closed shells, the paired state with $J = 0$ is by far the most favored; in this state, the two particles exert an isotropic pressure on the nuclear surface and the nucleus remains spherical. For a few pairs outside closed shells, the pairing continues to provide the dominant correlation. However, the energy gain associated with pair correlation increases linearly with n, the number of particles outside closed shells, while the energy associated with the creation of a deformation in the mean field grows as n^2, since the deformation increases linearly with n, and each of these n particles can experience an energy decrease that is proportional to the deformation (as long as the Pauli principle does not force particles into orbits with unfavorable anisotopies). Thus, with sufficiently many particles outside closed shells, the deformation can win and destroy the spherical symmetry preferred by the pairing.

In fact, the increasing role of deformation is visible in the spectra of spherical nuclei since as we go away from closed shells, the system becomes less and less stable against quadrupole shape fluctuations and this is seen as a gradual decrease in the frequency of collective vibrational excitations which describe these fluctuations. (These vibrational modes can be treated by the Random Phase methods discussed by George Bertsch in his lectures at this summer school.)

Similarly, the pairing correlations are not destroyed by the occurrence of deformations since the observed deformations continue to generate potentials that are symmetric under time reversal, and thus the single-particle states ν, in such a potential, come in degenerate pairs (ν, $\bar{\nu}$). The two orbits in each pair will have identical density distributions (Kramers degeneracy), and provide a basis for pair correlations in the presence of interactions of the type (4.5), acting on the states in the deformed potential. The pairs will no longer be spherically symmetric since they are somewhat squashed by the deformed potential. All the other classical attributes of the paired coupling scheme are, however, preserved, as, for example, the odd–even binding effect, the gradual variation of orbital occupancy at the Fermi surface, etc. The magnitude of the pairing order parameter (Δ), is however somewhat reduced as compared with what it would have been in a spherical system, since the density of single-particle levels at the Fermi surface is somewhat reduced by the presence of the deformation.

Some of the features of the competition described above can be instructively studied in a highly schematized model involving pairing and deformation producing interactions in a degenerate single particle space. However, before entering the analysis of this model, I would like to spend a moment discussing the role and historic significance of schematic models in the development of understanding of

the nuclear many-body problem. The models are based on drastic simplifications of the degrees of freedom involved and the effective interactions that act within the chosen space. These schematizations are chosen so as to enforce a high degree of symmetry. Since group theoretical methods provide the rational tools for describing such symmetries, the exact solutions provided by these models are expressed in terms of the "additional" quantum numbers provided by the group representations. Two models of this type have played a major role in nuclear physics – Racah's seniority (pairing in a degenerate configuration) and Elliott's $SU(3)$ (separable quadrupole forces in a degenerate oscillator configuration) – but many other schematizations have been carefully analyzed and have played a role in the development. The most important contribution of these models (in my opinion) has been in the realm of clarification of conceptual issues; the crisp definition of wave functions describing a rotational band or a paired state (in the schematized models) provided inspiration for the development and testing of concepts that expressed the more universal aspects of the problems. At the same time, the exact solutions provide benchmarks against which approximation methods can be tested. Attempts have also been made to use model states of this kind as the starting point for a phenomenological parameterization of experimental spectra. However, in such an application the severe truncation of the degrees of freedom that are represented will inevitably set limits to the extent that real physical states can be described. The quantitative magnitude of these limitations is usually very difficult to control. Thus, in my opinion the phenomenological use of such models has a rather limited applicability. In any case the model that will be analyzed in this chapter will be so violently schematic that it will be quite clear that its significance is strictly confined to illustrating the qualitative manner in which deformations and pairing can compete with each other.

Now for a model that can be used to study the competition between pairing and deformation. The model is derived from one first considered by Lipkin [38] and is based on a space of 4Ω degenerate single-particle states in which each state ν is labeled by two quantum numbers i and τ: the quantum numbers i come in pairs $(i, \bar{i})$, each of which ranges over Ω values 1, 2, 3, ..., Ω while τ takes on two values, $\tau = 1$ and $\tau = 2$:

$$\nu = (i, \tau) \qquad i \text{ and } \bar{i} = 1, 2, \ldots, \Omega$$
$$\tau = 1 \text{ or } 2 \tag{6.1}$$

The Hamiltonian contains a term H_Q which represents the self-interaction of an internal polarization in which the orbits $\tau = 1$ and $\tau = 2$ are occupied with different probabilities,

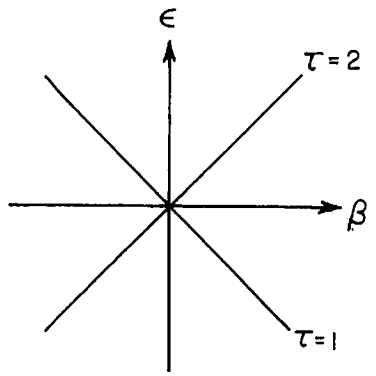

Fig. 38. Nilsson diagram for deformations in τ-space. The interaction (6.2) can be expressed in terms of a mean field that is proportional to the deformation in τ-space, $\beta \equiv (N_1 - N_2)$.

$$H_Q = -\kappa\,(N_1 - N_2)^2$$

$$N_\tau = \frac{1}{2}\sum a^+_{i\tau}a_{i\tau} + a^+_{\bar{i}\tau}a_{\bar{i}\tau} \tag{6.2}$$

In the presence of such an interaction, an asymmetry in the occupation of the $\tau = 1$ and $\tau = 2$ states generates a deformation in the mean field which tends to stabilize the asymmetry (see the Nilsson diagram drawn in Fig. 38). It should be emphasized that in this simple model the symmetry that is broken by a deformation in the τ-space is only the reflection symmetry ($(\tau = 1) \leftrightarrow (\tau = 2)$) and thus the collective mode in the presence of a deformation can only have two states rather than a rotational band.

In addition to the interaction (6.2), there is a pairing interaction in the Hamiltonian, which is color-blind to the τ quantum number,

$$H_{pair} = -G\left(A_1^+ + A_2^+\right)(A_1 + A_2)$$

$$A_\tau = \sum_{i=1}^{\Omega} a_{i\tau}a_{\bar{i}\tau} \tag{6.3}$$

The pairing interaction favors a wave function in which the pairs have equal amplitude for occupying all the available pair states, and this implies large fluctuations in the distribution of the particles between the two τ spaces. In contrast, the H_Q interaction favors a distribution in which all the particles are either in the $\tau = 1$ space or in $\tau = 2$. The model is thus the simplest possible system in which to study the competition between these two contrasting modes of correlation.

The exact solutions to the Hamiltonian

$$H = H_{Q+}H_{pair} \tag{6.4}$$

can be obtained by expanding in basis states characterized by definite numbers of pairs, N_τ, in each of the τ spaces

$$|N_1 N_2\rangle = \frac{1}{\Omega!}\sqrt{\frac{(\Omega - N_1)!\,(\Omega - N_2)!}{N_1! \cdot N_2!}}\,\left(A_1^+\right)^{N_1}\left(A_2^+\right)^{N_2}\,|\,0\,\rangle \tag{6.5}$$

The matrix elements of (6.5) can be easily evaluated by employing the commutation relations

$$\left[A_{\tau'}, A_\tau^+\right] = \delta(\tau, \tau')\,(\Omega - 2N_\tau) \tag{6.6}$$

which follow from the elementary anti-commutation relations for the Fermion operator $a_{i\tau}^+$ and $a_{i\tau}$. Thus,

$$\langle N_1 N_2|H_{pair}|N_1 N_2\rangle = -G\,\{N_1\,(\Omega - N_1 + 1) + N_2\,(\Omega - N_2 + 1)\} \tag{6.7a}$$

$$\langle N_1 + 1\;\; N_2 - 1\,|\,H_{pair}\,|\,N_1 N_2\rangle = -G\sqrt{(N_1 + 1)\,(\Omega - N_1)\,N_2\,(\Omega - N_2 + 1)} \tag{6.7b}$$

which leads to a bi-diagonal matrix of dimension $(N + 1) \times (N + 1)$, where N is the total number of pairs in the state considered.

$$N = N_1 + N_2 \tag{6.8}$$

The numerical diagonalization of such a matrix is a fairly simple matter even for rather large particle numbers, but the significant features of the spectra are, perhaps, more easily recognized in solutions that directly exploit the classical pictures that emerge in the limit of large quantum numbers. The eigenstates described above can be written

$$|\,N, \alpha\rangle = \sum_{m=-N}^{N} C_{N\alpha}(m)\,|\,N, m\rangle \tag{6.9}$$

where the quantum number α characterizes the different eigenstates which are constructed as a superposition of basis states characterized by the quantum number,

$$m = N_1 - N_2 \tag{6.10}$$

For systems with many particles, $N \gg 1$, the wave functions of low-lying states will vary smoothly with m, which can be considered as an almost continuous deformation variable describing motion in the collective space characterizing the

distribution of particles between the two τ-spaces. The potential energy controlling these fluctuations is obtained from the diagonal matrix elements (6.2) and (6.7a), to which the non-diagonal matrix elements of H_{pair} also make a contribution equal to (6.7b),

$$V(m) = -\kappa m^2 - G\frac{1}{2}\left\{-m^2 + \sqrt{\left(N^2 - m^2\right)\left[(2\Omega - N)^2 - m^2\right]}\right\} \tag{6.11}$$

where constant terms have been dropped, since they do not effect the spectrum or the structure of the eigenstates, and the square root term has been somewhat simplified by neglecting terms of relative order N^{-1} or Ω^{-1}. It is seen that for relatively small values of N, the square root term dominates and favors the region around $m = 0$, where there are comparable numbers of particles in the $\tau = 1$ and $\tau = 2$ states. This corresponds to the dominance of pairing for configurations near to closed shells, as discussed qualitatively above. With increasing N, the $m = 0$ region becomes less and less stable until, at a critical value,

$$N^* = \Omega\left\{1 - \sqrt{1 - \frac{G}{\kappa}}\right\} \tag{6.12}$$

the non-deformed state $m = 0$ becomes unstable, and for larger values of N, the ground state exhibits a deformed shape. Fig. 39 sketches the m dependence of the potential (6.11) for several different values of N. The onset of deformation in the wave function is signaled by the appearance of close doublets in the spectrum, as shown in Fig. 40. These doublets are all that is left of the collective "band" since in this model, the deformation breaks only a discrete symmetry* i.e. the invariance of H with respect to $(\tau = 1) \leftrightarrow (\tau = 2)$. The deformations can only occur if $\kappa > G$, but if this condition is satisfied, there will be a region around mid-shell where the system exhibits deformation and associated doublet structures

* A generalization of the model considered here has been analyzed by Vassanji et al. [39]. The deformation producing interaction, H_Q, in this generalization is constructed so that it is invariant under two-dimensional rotations. In the deformed phase, this model then yields rotational bands with many states having different angular momenta.

The model considered in the text and the generalization can be characterized by the group theoretical symmetries which make exact solutions possible. The model defined by (6.3) and (6.2) is invariant under $SU(2) \times SU(2)$, which involves the six operators N_τ, A_τ^+, and A_τ, while the more general version considered by Vassanji et al. involves four more generators:

$$A_{12} = \sum_{i=1}^{a} a_{i1}a_{\bar{i}2} \qquad A_{12}^+ = (A_{12})^+$$

$$A_{21} = \sum a_{i2}a_{\bar{i}1} \qquad A_{21}^+ = (A_{21})^+$$

and is invariant under an $SO(5)$ group.

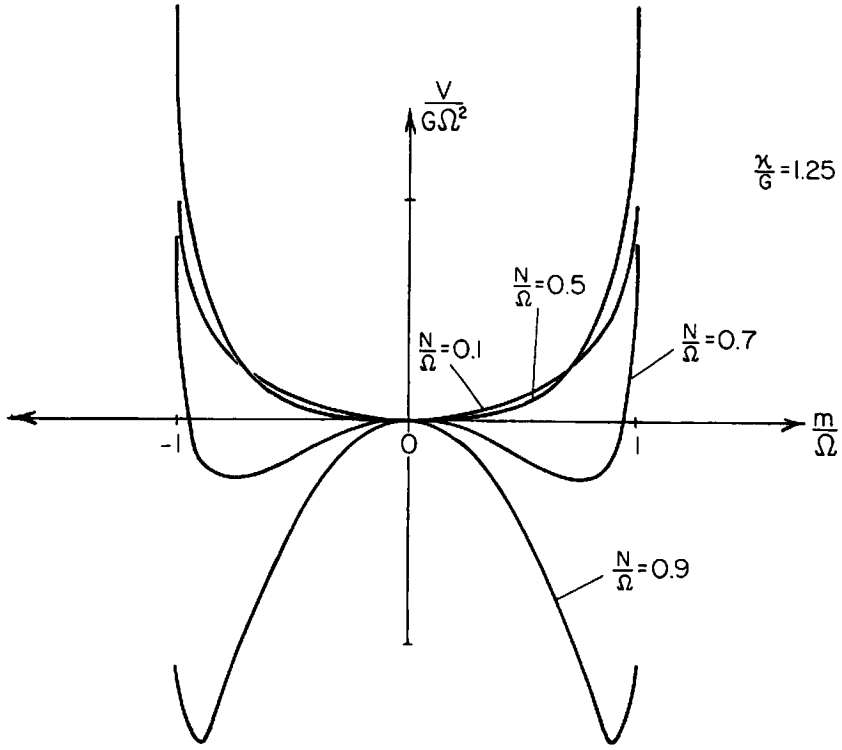

Fig. 39. Potential energy as a function of $N_1 - N_2$. The function (6.11) is plotted for four different values of the particle number N, with $\kappa/G = 1.25$ in each case. For this value of κ/G the critical value of $(N/\Omega)^* = 0.555$.

in the low-energy spectrum. For $N < N^*$, vibrations in the deformation coordinate are responsible for the lowest excitations, which have decreasing energy as the particle number increases. In the region of the transition to static deformation, the vibrations have come down to a frequency that is of the order of $\Omega^{-1/3}$ compared with the frequency in the closed shell region (see Fig. 40). In the deformed phase, the lowest excitation corresponds to the "Goldstone doublet", while the remaining low-energy excitations in Fig. 40 correspond to collective vibrations around the deformed equilibrium shape.

The qualitative patterns of the observed low-energy excitations in nuclei follow rather closely those derived above, with, of course, appropriate differences in the details of the quantum numbers reflecting the oversimplified geometry of the model system. An example of the dependence on particle number of the compe-

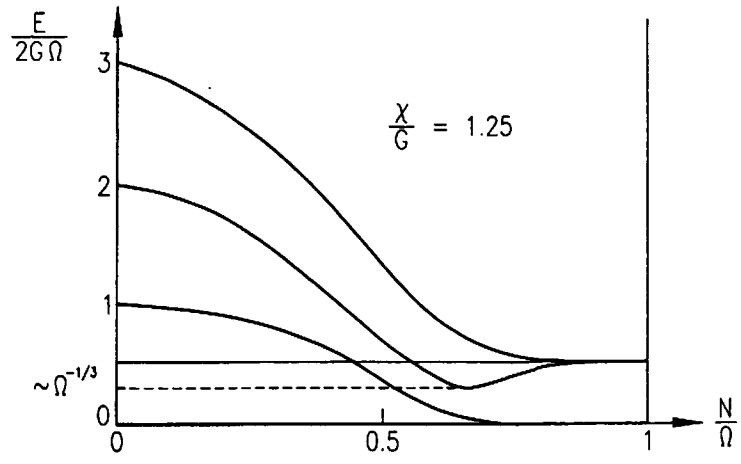

Fig. 40. Energy spectrum as function of particle number. For $N \ll \Omega$ the collective excitations correspond to small amplitude vibrations in the approximately harmonic potential plotted in Fig. 39. With increasing particle number, the restoring force for these vibrations becomes softer and the frequency decreases until the symmetric equilibrium becomes unstable. For particle numbers beyond the instability point the collective excitations become organized into doublets corresponding to the almost independent oscillations around the two separated non-zero equilibrium points.

tition between pairing and quadrupole deformation is provided by Fig. 41, which shows the spectra of samarium isotopes ranging from spherical $^{144}_{62}$Sm with a closed shell configuration for the neutrons ($N = 82$) to the strongly deformed $^{154}_{62}$Sm with $N = 94$.

7. High-spin states and super deformation

The investigation of nuclear reactions initiated by accelerated beams of heavy nuclei (extensively developed during the 1970's) has made possible the study of nuclear states with very high angular momentum. These studies have provided very detailed spectroscopic results, addressing such questions as the response of the independent particle dynamics to the Coriolis and centrifugal forces resulting from nuclear rotation, and the development of appropriate concepts for describing the effect of such rotation on pair correlations and collective deformation. The present chapter cannot present more than a brief survey of some of the most striking and important discoveries that have been made on this new frontier of nuclear structure.

The first issue that we shall examine concerns the scope of the new field; how

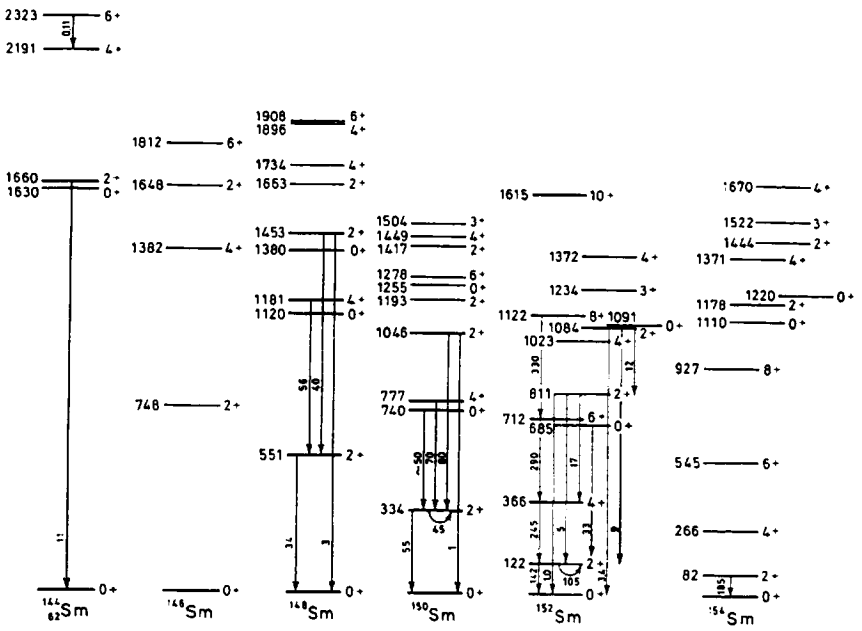

Fig. 41. Experimentally observed low energy spectra for even-A samarium isotopes ($Z = 62$). The figure illustrates the changing low energy excitations associated with the competition between the pairing and quadrupole deformations as a function of the number of particles in open shells. In ^{144}Sm with a neutron closed shell ($N = 82$), the lowest energy $I\pi = 2+$ state occurs at 1.66 MeV, comparable to the energy involved in creating a broken pair of protons (See Fig. 27 for proton pairing energies). With increasing neutron number the energy of the first excited 2+ state decreases reflecting the decreasing strength of the restoring force for quadrupole shape vibrations. These vibrations obey Bose statistics since they are built out of two quasi-particle excitations (broken pairs) and thus for $N_2 = 2$ (two quadrupole quanta) we expect $I\pi = 0, 2, 4+$ and $N_2 = 3$; $I\pi = 0, 2, 3, 4, 6+$. The incipient formation of these multiplets can be seen in the low energy spectra of ^{148}Sm and ^{150}Sm. However, unharmonicities in the spectra are also becoming significant as we approach the transition (apparently occurring between ^{150}Sm and ^{152}Sm) from spherical to quadrupole deformed equilibrium shape. Starting at ^{152}Sm the low energy spectrum can be rather well described in terms of rotational bands built on intrinsic states having axially symmetric quadrupole deformed shapes. The figure is taken from [25].

much angular momentum can be put into a nuclear system before it is destroyed by internal instabilities, or the angular momentum is disposed of by the ejection of particles carrying large orbital angular momentum. In most cases, the limit is set by the fission instability, i.e. with increasing rotational frequency the centrifugal force drives the nucleus into more and more elongated shapes which eventually are torn apart into two fragments at a critical angular momentum, I_{crit}. The magnitude

of the critical angular momentum can be simply estimated on the basis of the liquid drop model. In this model, the energy of the nucleus in the neighborhood of the spherical shape, $\beta = 0$, and including the effect of an angular momentum, I, is described by

$$H = \frac{\hbar^2 I^2}{2\mathcal{J}(\beta)} + V(\beta) \tag{7.1a}$$

$$V(\beta) = V(0) + \frac{1}{2}C\beta^2 + \cdots \tag{7.1b}$$

where the rotational energy is determined by the moment of inertia, $\mathcal{J}(\beta)$. As discussed in Chapter 5, the nuclear moments of inertia scale approximately like the moments of a rigid body, which implies $\mathcal{J} \sim AM_pR^2 \sim A^{5/3}$. The rigid moment also depends on deformations with a term that, to leading order, is linear in β. The non-rotating liquid drop has a spherical shape and the restoring force, C, receives contributions from the surface tension (proportional to the area of the surface $\sim A^{2/3}$) and a negative term from the Coulomb energy ($\sim Z^2/A^{1/3}$). The quantitative prediction of the fission instability involves higher-order terms than those represented in (7.1), but quite generally the critical angular momentum occurs for a state in which the rotational and restoring force terms have comparable magnitude, and thus

$$I_{crit} \sim (\mathcal{J}/C)^{1/2} \sim A^{7/6}\hbar f\left(\frac{Z^2}{A}\right) \tag{7.2}$$

where the last factor, $f(Z^2/A)$, describes the correction to the pure surface tension term resulting from the Coulomb energy. For $Z^2/A = 0$ $f = 1$ (by definition); for $Z^2/A = (Z^2/A)_{crit} \approx 45$, the Coulomb energy is so large that even the non-rotating nucleus is unstable with respect to the fission mode and thus $f((Z^2/A)_{crit}) = 0$. The shapes, energies, and instabilities of rotating liquid drops have been systematically evaluated in a classic investigation by Cohen, Plasil and Swiatecki [40] and the values of the critical angular momentum from that work are given in Fig. 42. The attentive student will notice that all the qualitative numbers that characterize this figure are of order 10^2 (the maximum value of I_{crit}, the maximum value of Z for ground states with finite fission barriers, and the value of A for $(I_{crit})_{max}$); this circumstance reflects the fact that all these numbers are determined by the inverse of the fine-structure constant that measures the relative strength of the nuclear and the electrical forces.

A different view of the role of the fission instability on high-spin studies can be obtained from Fig. 43, which indicates several significant landmarks in a nuclear phase diagram that plots excitation energy, E, against angular momentum, I. The fission barrier – the excitation energy of the fission saddle point measured with

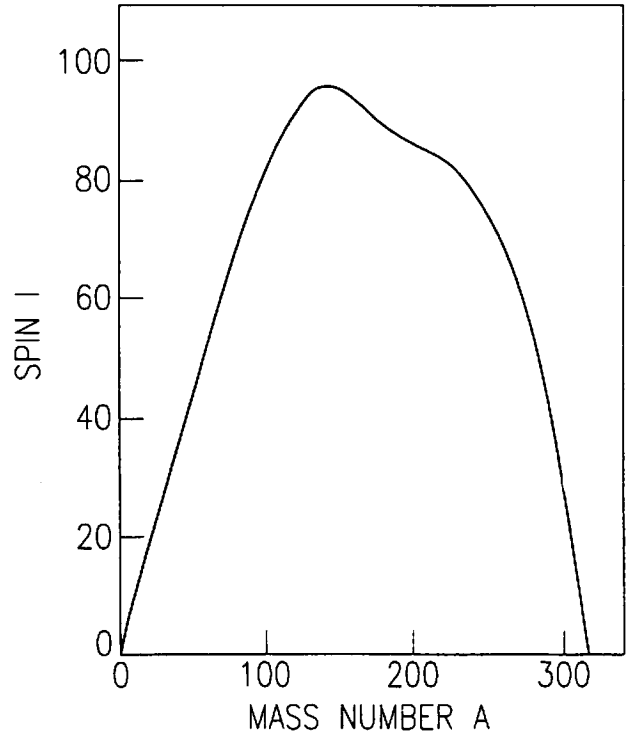

Fig. 42. I_{crit} as a function of mass number, A. The liquid drop estimate of the maximum value of the angular momentum, I, for which there is a locally) stable equilibrium shape is plotted as a function of the mass number, A. For each A, the charge number, Z, corresponds to the most stable isobar. The figure is based on Cohen et al. [40].

respect to the nuclear ground state – is labeled B_f. The yrast* line is the energy of the lowest state in the nucleus with a given angular momentum. Because the saddle point shapes are more elongated than the yrast shapes, the moment of inertia at the saddle point is greater than that at the yrast line, and thus B_f increases with I more slowly than the yrast line; at I_{crit}, the yrast and fission barrier are equal, and for $I > I_{crit}$, there are no stable nuclear shapes. Also included in Fig. 43 is the energy, S_n, necessary to remove a neutron (with angular momentum $l_n = 0$) from the nucleus. In a nuclear reaction that brings the system into states lying below both

* This synthetic term is constructed as the superlative of the Swedish "yr" meaning dizzy, and is universally used in the nuclear physics community. The particle physicists refer to the same concept as "the leading trajectory".

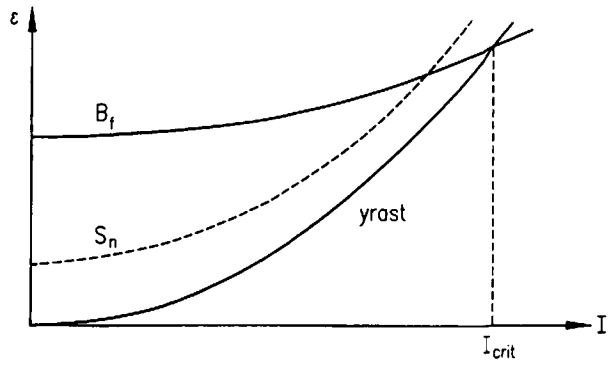

Fig. 43. Nuclear phase diagram, indicating stability limits as function of angular momentum, I. See discussion in text.

S_n and B_f, the only available decay mode is the emission of gamma rays; there will occur a cascade of such radiation, that cools the system toward the yrast line and radiates away the angular momentum. It is the detailed spectroscopic study of these radiative cascades that have provided almost all the available information on the structure of nuclei in high angular momentum states. Concerning the nature of the states that are studied in such processes, it is relevant to note that in the region near S_n, the detailed studies (at low angular momentum) have established the validity of the random matrix description (chaotic quantum structure; see Chapter 1) extending over intervals of 10 or more level spacings (for levels of the same spin and parity); by the time the system has cooled to excitation energies below 1 or 2 MeV above the yrast line, it is expected (and experimental data confirm) that the structure of the nuclear state has a similar order and simplicity as observed in the states with similar excitation energies with respect to the ground state. Thus, in near yrast states at $I \sim 50\hbar$, the total excitation energy may be of order 25 MeV, but this energy is tied up in the single degree of freedom associated with the angular momentum and thus the intrinsic degrees of freedom are practically at a temperature of $T = 0$.

Continuing the discussion of the qualitative features of the spectra in the yrast regions, we can ask about the nature of the nuclear degree of freedom involved in generating the very large angular momenta. The observed spectra in the region along and just above the yrast line can be interpreted in terms of two sharply distinguished modes for systematically generating angular momentum:

(i) Collective rotation

Collective rotational bands exhibiting the properties discussed in Chapter 5 (see Fig. 37) are observed in the yrast regions of many nuclei. These structures are

attributed to the existence of an intrinsic anisotropy in the nuclear density, * and the states that belong together in the band are linked by strongly enhanced $E2$ transitions, which provide a quantitative measure of the intrinsic anisotropy (see Table 4). The low-lying intrinsic states in the neighborhood of the yrast line can be assigned quantum numbers that reflect the occupancy of the single-particle states associated with the motion of the nucleons in the intrinsic anisotropic mean field. There is a rotational band associated with each such intrinsic state.

(ii) Aligned coupling scheme

An alternative to collective rotation is provided by the possibility of successively aligning the angular momentum, j_i, of single nucleons along the direction defined by the total angular momentum I. This mode of systematic angular momentum generation occurs when the nuclear mean field has axial symmetry with respect to the axis of alignment defined by I; this condition ensures the absence of collective rotation about this axis, and at the same time implies the existence of a conserved quantum number, Ω_i, characterizing the component of the single-particle angular momentum along the symmetry axis. In this coupling scheme, the total angular momentum is built up as the sum of the (quantized) contributions from the occupied single-particle states:

$$I = \sum_{\substack{\text{occupied} \\ \text{orbits}}} \Omega_i \tag{7.3}$$

The structure of the yrast line associated with this "aligned" coupling scheme is dramatically different from that resulting from collective rotation. The energy of the yrast transitions fluctuates wildly since it depends on the energy differences of the single-particle states involved in the transition of a particle from one orbit (Ωi) into another (unoccupied) orbit with a larger value of Ω_i. Similarly, the transition matrix elements for these transitions along the yrast line will not be of collective nature, but rather will often be strongly hindered by single-particle selection rules applying to the involved one-particle states. Isomerism (delayed transitions) occurs as a frequent feature of the γ-ray cascade along the yrast line of a nucleus characterized by the aligned coupling scheme. We can also express these features by noting that the axial symmetry of the mean field implies that there are no forces acting to establish coherence between the different particles moving in this potential. Thus, the fluctuations in density and current that are responsible for electromagnetic radiations are the result of incoherent contributions from the separate particles. The contrasting yrast patterns associated with collective rotation

* The anisotropic element does not strictly have to be related to the density, and in fact it has been possible in a few cases to identify rotational bands in nuclei associated with collective anisotropies in the intrinsic current distribution ([41] and references therein). In these bands, there occurs regular sequences of angular momentum and energy, but the states are not linked by strong $E2$ matrix elements; rather, enhanced $M1$ matrix elements reveal the nature of the intrinsic anisotropy.

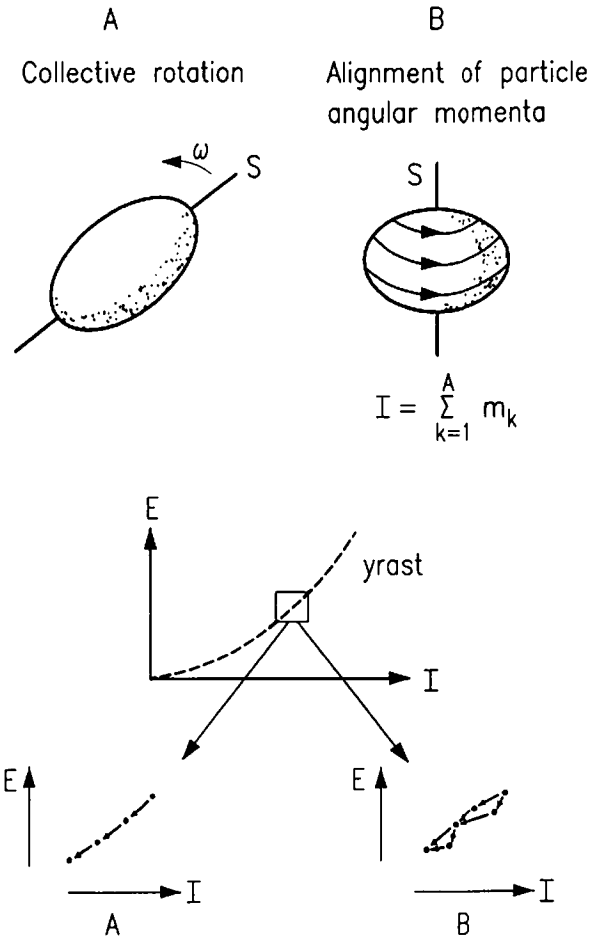

Fig. 44. Two modes for building angular momentum in atomic nuclei.

and single-particle alignment are summarized in the schematic Fig. 44 and in the comparison of the experimental spectra in Figs. 37 and 45.

7.1. *Super deformation*

In Chapter 5, we considered the collective anisotropies that occur in the shapes of low-lying nuclear states as a result of the stresses associated with singe-particle orbits in partially filled shells. We found that these stresses imply deformations that

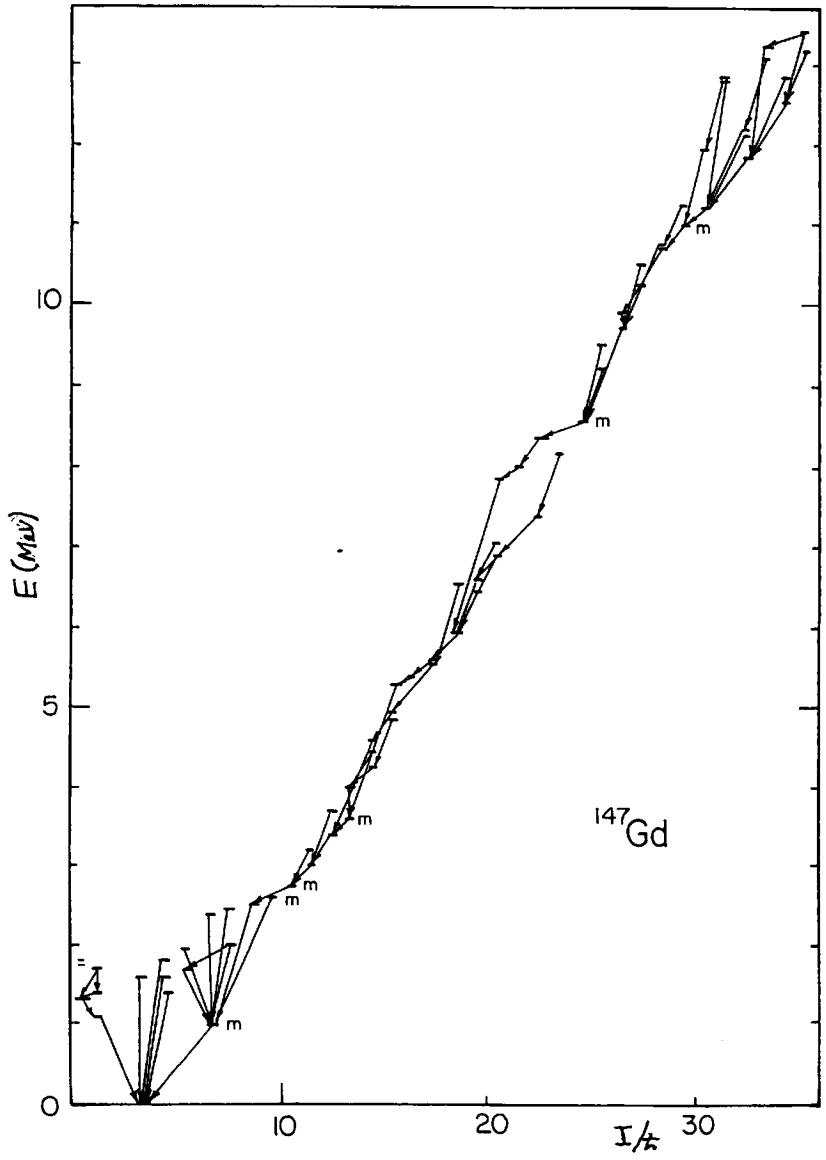

Fig. 45. Yrast region for the spectrum of ^{147}Gd. The arrows indicate observed γ-ray transition connecting the near-yrast states. The irregular pattern of energies and transitions is characteristic of the build-up of angular momentum by the alignment of angular momentum of independent nucleons.

are fundamentally small (eccentricities of order $A^{-1/3}$). In the present section, we shall consider eccentricities that are of order unity, and thus are generated by mechanisms that are significantly different from those involved in the small ground-state deformations. The large deformations can only occur* in the presence of "external" forces that favor the deformed shapes (such forces are provided by the nuclear Coulomb energy which endows the elongated fission saddle-point shape with an (unstable) equilibrium and the rotational energy which can also favor an elongated shape for sufficiently large angular momentum). Even in the presence of these forces, the highly deformed shapes would be unstable except for the presence of an appreciable contribution from the shell structure which, as we shall see, can favor certain discrete values of the eccentricity. In order to find these special shapes, we can attempt to exploit the analysis presented in Chapter 3, which exhibits the connection of shell structure to the occurrence of degenerate families of periodic classical orbits in the appropriate potentials. Thus, we must attempt to find strongly anisotropic potentials that are capable of generating such orbits. This is in general a difficult task, but very useful guidance is provided by the study of spectra and orbits of particles in an anisotropic harmonic oscillator potential:

$$H = \frac{1}{2M}p^2 + \frac{1}{2}M\left\{\omega_x^2 x^2 + \omega_y^2 y^2 + \omega_z^2 z^2\right\} \tag{7.4}$$

We shall confine the discussion to potentials with axial symmetry, which can be described by a single deformation parameter, δ, as described by (5.7) and (5.8). Thus,

$$E(n_x n_y n_z) = \hbar\bar{\omega}\left\{N + \tfrac{3}{2} - \tfrac{1}{3}\delta(2n_z - n_x - n_y)\right\}$$

$$N = n_x + n_y + n_z \tag{7.5}$$

For $\delta = 0$, the potential (7.4) is isotropic, and all the classical orbits are planar ellipses with ratio of radial to angular frequencies $\omega_r : \omega_l = 2 : 1$. This leads to the familiar quantal spectrum (see Fig. 46) with degeneracies so that the closed shells correspond to particle numbers $\mathcal{N} = 2, 8, 20, 40, 70, \ldots$ (including the twofold degeneracies resulting from the spin of the nucleon). For non-zero values of δ, these degeneracies are partially removed and indeed, for general (irrational) ratios of the oscillator frequencies, there are no closed orbits and no degeneracies in the spectrum. However, for the special case of rational ratios of the frequencies

$$\omega_\perp : \omega_z = a : b \qquad (a \text{ and } b = \text{integers}) \tag{7.6}$$

* In the present context, the word "occur" means "to have a sufficient local stability so that distinct quantum states associated with these shapes can be found in the nuclear spectra".

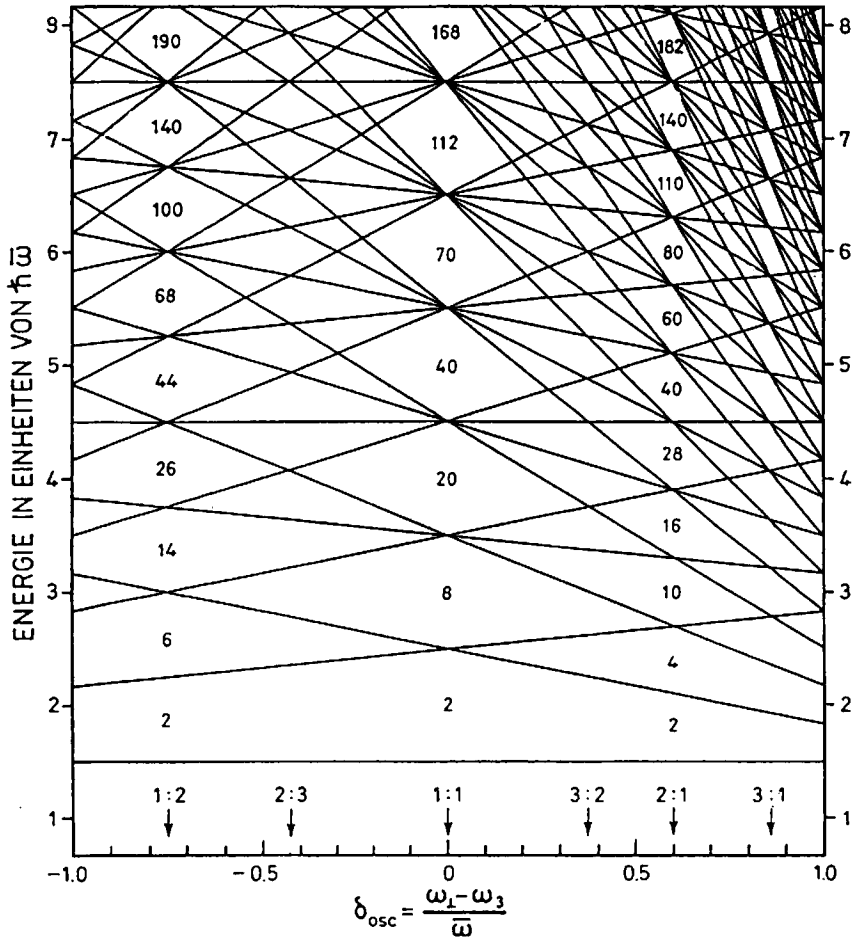

Fig. 46. Single-particle spectrum for axially symmetric harmonic oscillator potentials. The figure is taken from [25, p. 592].

the orbits do close after a rotations about the z axis and b oscillations along this axis; the quantal spectra exhibit new patterns of degeneracies associated with these families of periodic orbits. The shorter the period of the orbit, the greater the

degeneracies associated with it, and thus special interest * attaches to

$$a : b = 2 : 1 \tag{7.10}$$

which has acquired the, perhaps overly dramatic, name "super deformation".

The classical orbits in the 2 : 1 potential depend on the relative phases of the motion in the axial and perpendicular directions and, as sketched in Fig. 47, can vary from a figure eight to a bent-banana shape. The particle numbers corresponding to closed shells in this potential are

$$\mathcal{N} = 2, 4, 10, 16, 28, 40, 60, 80, 110, 140, \ldots \tag{7.11}$$

As with the closed shells in heavier spherical nuclei, the closed shells in super deformed nuclei usually occur at particle numbers a few units greater than those predicted by the harmonic oscillator, reflecting the more sharply defined surface of the true nuclear potential and the effect of the spin-orbit force.

The first examples of super deformed states in nuclei were provided by the observation of isomeric states in heavy nuclei that decay by spontaneous fission with astonishingly short half-lives [42]; for example, $^{241}_{95}$Am in its ground state has a spontaneous fission half-life of 1.0×10^{10} yr, which is quite typical for nuclei in this region of the periodic table; in this same nucleus, there is an isomeric state that decays predominantly by spontaneous fission with a half-life of 1.2×10^{-6} s. At the present time, more than 40 examples of such "fission isomers" have been

* The next most elementary degeneracies are expected for $(a, b) = (3, 1)$, which has not yet been observed with certainty but is widely referred to in the literature as "hyper deformation".

The attentive student may be wondering why we do not address equal interest to the shell structure in the oblate shapes with rationally related frequencies; for example $(a, b) = (1, 2)$. Indeed, the latter shape exhibits shell structures with degeneracies that are even greater than those in the (2, 1) shape, as can be seen directly by counting the degeneracies in Fig. 46 or by calculating the periods, T, of the corresponding classical orbits

$$T(2, 1) = (2)^{2/3} T(1, 2) \tag{7.7}$$

The absolute values of the oscillator frequencies at different shapes have been normalized by assuming that the equi-potential surfaces enclose a volume of space that is independent of deformation, and thus

$$\omega_\perp^2 \omega_z = \text{constant} \tag{7.8}$$

Despite the larger shell structure energies expected at the (1, 2) shape, these configurations are not expected to give rise to yrast states at high angular momentum because the moments of inertia of these oblate shapes (for rotations about an axis perpendicular to the symmetry axis) are significantly less than for the prolate shapes:

$$\mathcal{J}(2, 1) = 1.57 \mathcal{J}(\beta = 0)$$

$$\mathcal{J}(1, 2) = 0.99 \mathcal{J}(\beta = 0) \tag{7.9}$$

and thus the rotational energy of the (1, 2) shape is expected to be about equal to that of the spherical shape for the same angular momentum.

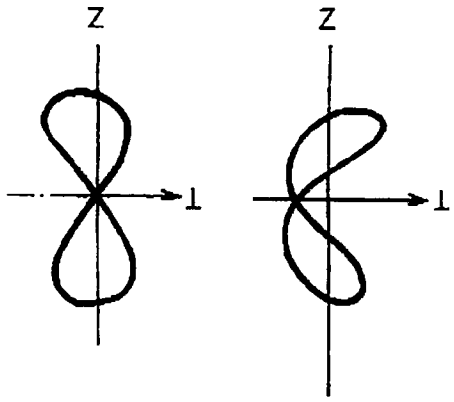

Fig. 47. Illustrative shapes from the family of degenerate classical orbits occurring for an axially symmetric harmonic oscillator potential with ratio of frequencies, $\omega_\perp : \omega_z = 2 : 1$.

found in nuclei in the region from $^{233}_{90}$Th to $^{245}_{97}$Bk (see the Table of Superdeformed Nuclear Bands and Fission Isomers, by B. Singh et al. [43]) The occurrence of these very fast spontaneous fission rates (together with many other properties of these states) can be understood from the schematic diagram of the nuclear potential energy surface sketched in Fig. 48. The potential energy function has its lowest point at the shape corresponding to the nuclear ground state, increases with deformation as one goes away from this minimum, but then bends over at the fission saddle point, which is typically about 5 or 6 MeV above the ground state in heavy nuclei, and then decreases as the Coulomb force drives the system toward sission. In nuclei exhibiting the fission isomer phenomenon, the potential energy function has a more complicated structure, with a second minimum in the region of shapes that would have been the saddle point in a "normal" nucleus. The second minimum is created by the shell structure which strongly favors the 2 : 1 shape when the particle numbers are in the region of those appropriate for a closed-shell configuration in this shape. The short lifetimes of the fission isomers result from the much reduced barrier that must be penetrated in escaping from the second minimum as compared with that for escaping from the ground state. The observed fission lifetimes define the neutron number $N = 144$ or 146 as that characterizing the closed-shell configuration, in good agreement with the expected small corrections to the number $N = 140$ predicted by the harmonic oscillator potential [44].

In a few nuclei (^{236}U, ^{238}U, ^{239}Pu, and ^{240}Pu), it has been possible to observe rotational bands associated with the fission isomer states. The rotational energies in these bands are described by moments of inertia that are much larger than those

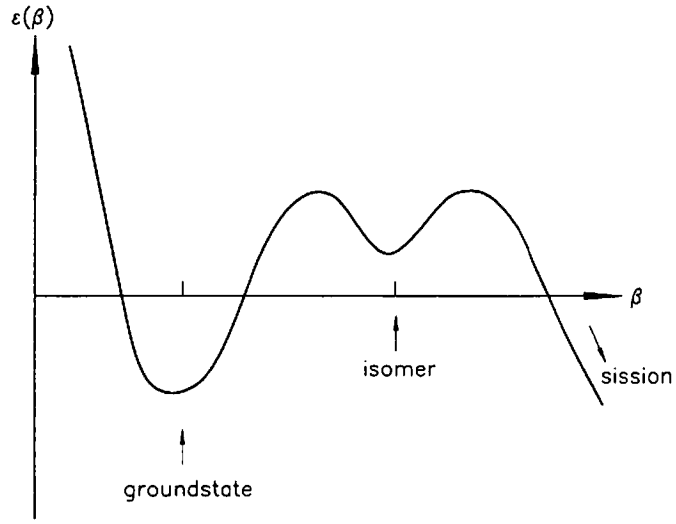

Fig. 48. Potential energy as function of deformation for a nucleus for which there is a second minimum along the path to fission.

of the ground state band, as expected from the large deformation (see Eq. (7.9)). The value of the deformation can be determined from the $E2$ matrix elements for gamma transitions between states in these rotational bands; the measured values confirm that the shapes correspond to a ratio of axes of 2 : 1.

The study of the structure of nuclei with super deformation has been vastly expanded during the past ten years by the discovery of long sequences of rotational states at high angular momentum in many nuclei with neutron and proton particle numbers in the neighborhood of the closed shells defined by Eq. (7.11). At present, over 130 such rotational bands have been experimentally identified in three different regions of the periodic table [43]:

$$\begin{aligned} &A \approx 84 \quad (Z \approx 40 \quad N \approx 44) \\ &A \approx 148 \quad (A \approx 64 \quad N \approx 84) \\ &A \approx 194 \quad (Z \approx 80 \quad N \approx 114) \end{aligned} \tag{7.12}$$

These bands are populated in reactions in which two heavy nuclei with relative kinetic energy somewhat above the Coulomb barrier collide and form a compound nucleus. The angular momentum of this system can, depending on the impact parameter, be anywhere in the range from $I = 0$ up to the limiting value I_{max} set by the fission instability. As described in the lectures by G. Sletten, the neutron evaporation and subsequent gamma emission processes eventually populate states

in the neighborhood of the yrast line, and if the yrast states involve configurations that live in the super deformed minimum, the possibility exists for detailed spectroscopic investigation of these configurations. To exploit this possibility, however, requires very considerable experimental sophistication since the interesting transitions between states in the super deformed bands occur in the presence of an enormous background of gamma rays from other decay products of the initially formed compound nucleus. The discrimination against this background is very powerfully assisted by the fact that, within the super deformed bands, the energies of the quantum states follow quite accurately the pattern described by a rigid rotator,

$$E_{rot} = \frac{\hbar^2}{2\mathcal{J}} I(I+1) \tag{7.13}$$

which implies that the gamma ray energies are

$$E_\gamma(I \to I-2) = \left(\frac{\hbar^2}{2\mathcal{J}}\right) 2(2I-1) \tag{7.14}$$

which yields, for the difference between gamma ray energies in the same band,

$$E_\gamma(I \to I-2) - E_\gamma(I-2n \to I-2n-2) = \frac{\hbar^2}{2\mathcal{J}} \cdot 8n \tag{7.15}$$

The fact that these differences are integer multiples of a common unit that is independent of I, opens the possibility of searching in the hopelessly unresolved total spectrum of gamma rays for sequences of transitions that are in coincidence with each other, and at the same time exhibit the integer relationships of energy differences. Such searches have been wonderfully successful and have provided the starting point for the detailed studies of the many super deformed rotational bands referred to above (an example is shown in Fig. 49.

The observation of these long sequences of rotational transitions in many different bands in the same or neighboring nuclei provides a rich body of spectroscopic evidence that opens the possibility of addressing many important questions concerning the structure of these systems. This is not the place to begin a review of these fascinating new data, but rather I would like to end with a brief sampling of some of the general issues that have become accessible as a result of these studies:

1. How do these bands get populated from the higher lying states formed initially in the fusion reactions?

2. The classification and interpretation of the different intrinsic states responsible for the many rotational bands built on super deformed configurations. At present as many as nine different superdeformed rotational bands have been identified in a single nucleus ($^{148}_{63}Eu_{85}$).

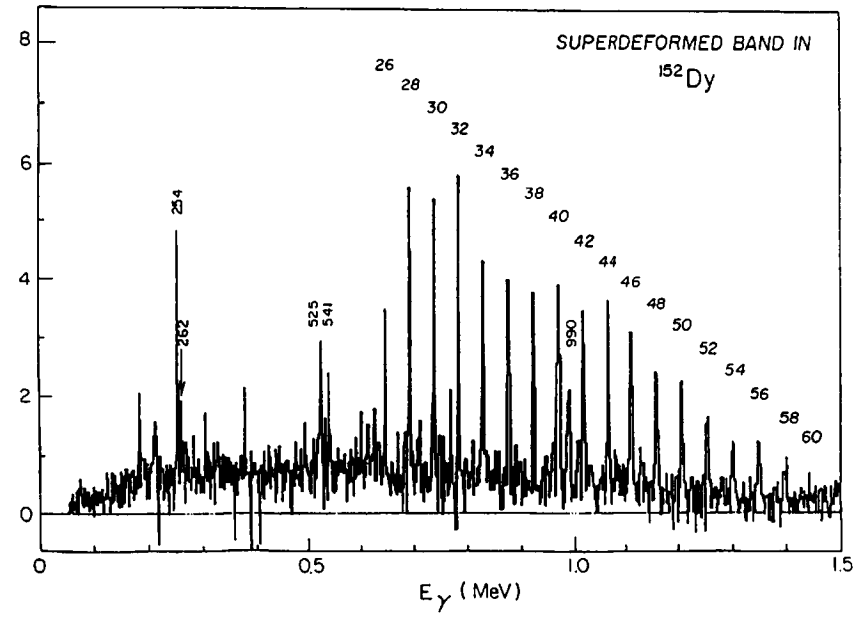

Fig. 49. Gamma ray spectrum indicating the occurrence of a super-deformed rotational band in the nucleus, ^{152}Dy. The experiment on which this figure is based [48] represented the first observation of such a long, regular sequence of coincident γ-rays. There are now (1997) over 200 different bands of similar type known in nuclei ranging from $A \approx 60$ to $A \approx 200$. In all these observations the neutron and proton numbers can be related to the sequence (7.11) that characterizes closed shells in an axially symmetric potential with ratio of axes 2 : 1.

3. Are there collective vibrational fluctuations in the nuclear shape with respect to the super deformed equilibrium, and if so, which shape degrees of freedom are involved?

4. What is the role of pairing in these highly deformed, rapidly rotating systems?

5. Is it possible to identify new, velocity-dependent terms in the mean field that determine the single-particle orbits?

6. Are there other broken symmetries in these exotic nuclear configurations and if so, how will they be manifest in the spectra?

7. Going to higher excitation energies above the yrast line, how can one observe and characterize the expected transitions from low-energy order to high-energy chaos in the nuclear dynamics?

8. What determines the angular momentum at which super deformed bands decay into normally deformed states and how can these transitions be characterized?; does pairing play a role?

References

[1] A. Bohr and B.R. Mottelson, Nuclear Structure Vol. I (W.A. Benjamin, 1969).
[2] O. Bohigas, Les Houches Session LII, 1989 (Elsevier, Amsterdam, 1991).
[3] T.A. Brody, J. Flores, J.B. French, P.A. Mello, A. Pandey, and S.S.M. Wong, Rev. Mod. Phys. 53 (1981) 385.
[4] A.D. Stone, P.A. Mello, K. Muttalib, and J.L. Pichard, in: Altschuler, Lee and Webb, eds., *Mesoscopic Phenomena in Solids* (North Holland, 1991).
[5] J.D. Garrett, J.Q. Robinson, A.J. Foglia, and H.Q. Lin, Phys. Lett. B392 (1997) 24.
[6] M.G. Mayer, Phys. Rev. 74 (1948) 235.
[7] M.G. Mayer, Phys.Rev. 75 (1949) 1969.
[8] O.Haxel, J.H.D. Jensen, and H.E. Suess, Phys. Rev. 75 (1949) 1766.
[9] L.H. Nosanov, J. Low Temp. Phys. 23 (1976) 613.
[10] J. de Boer, *Prog. in Low Temp Phys II* (North Holland, 1957).
[11] J. de Boer, Physica 14 (1948) 139.
[12] J. de Boer and R.J. Lundbeck, Physica 14 (1948) 520.
[13] R.B. Wiringa et al., Phys. Rev. C29 (1984) 1207.
[14] L.D.Landau, Sov. Phys. JETP 3 (1957) 920 and 5 101.
[15] Ph. Nozières, *Theory of Interacting Systems* (Benjamin, NY, 1964).
[16] P.W. Anderson, *Basic Notions of Condensed Matter Physics* (Benjamin, 1984).
[17] A.B. Migdal, Nucl. Phys. 13 (1959) 655.
[18] V.R. Pandiharipande, I. Sick, and K.A. de Witt Huberts, Rev. Mod. Phys. 69 (1997) 981.
[19] N. Bogoliubov, J. Phys. (USSR) 11 (1947) 23.
[20] S.T. Beliaev, Mat. Fys. Medd. Dan. Vid. Selk. 32 (11) (1959).
[21] R.P. Feynman, Phys. Rev. 91 (1953) 1301.
[22] S. Fantoni, private communication, 1996
[23] R. Balian and C. Bloch, Ann. Phys. 69 (1972) 76.
[24] M.C. Gutzwiller, J. Math. Phys. 12 (1971) 343.
[25] A. Bohr and B.R. Mottelson, *Nuclear Structure Vol. II* (W.A. Benjamin, 1969).
[26] H. Goldstein, *Classical Mechanics* (1974) p. 288 ff.
[27] M.V. Berry and M. Tabor, J. Phys. A10 (1977) 373.
[28] P.M. Morse and H. Feshbach, *Methods of Math. Phys.* (McGraw-Hill, 1953) p. 466.
[29] M. Brack, Rev. Mod. Phys. 65 (1993) 677.
[30] G. Racah, Farkas Memorial Volume (1952) 294.
[31] H.A. Bethe and R.F. Bacher, Rev. Mod. Phys. 8, (1936) 82.
[32] P. Vogel, B. Jonson, and P.G. Hansen, Phys. Lett. 139B (1984) 227.
[33] N. Bohr, Studier over Metallernes Elektrontheori, Dissertation, Thaning og Appel, Copenhagen (1911); translated in Niels Bohr, *Collected Works*, Vol. 1 (North Holland, 1972) p. 291.
[34] L.D. Landau and E.M. Lifshitz, *Quantum Mechanics, Non-Relativistic Theory* (Pergamon Press, 1977) p. 405 ff.
[35] G. Delacrétaz et al., Phys. Rev. Lett. 56 (1986) 2598.
[36] P.A. Butler and W. Nazarewicz, Revs. Mod. Phys. 68, 349 (1996)
[37] I. Hamamoto, B. Mottelson, H. Xie, and X.Z. Zhang, Z. Phys D21 (1991) 163.
[38] H. Lipkin, *Lie Groups for Pedestrians* (North-Holland, 1965).
[39] M.G. Vassanji, Á. Klein, and C. Dasso, Phys. Rev. C17 (1978) 755.
[40] S. Cohen, F. Plasil, and W. Swiatecki, Ann. Phys. 82 (1974) 557.
[41] S. Frauendorf, Nucl. Phys. A557 (1993) 259c.
[42] S.M. Polikanov et al., J. Exp. Theor. Phys. (USSR) 42 (1962) 1464.

[43] B. Singh, R.B. Firestone, and S.Y.F. Chu, *Table of Superdeformed Nuclear Bands and Fission Isomers*, LBL 38004, (Lawrence Berkeley Laboratory, 1996).
[44] S. Bjørnholm and J.E. Lynn, Rev. Mod. Phys. 52 (1980) 725.
[45] N. Bohr, Nature 137 (1936) 344.
[46] H.I. Liou et al., Phys. Rev. C5 (1972) 974.
[47] R.B. Firestone, *Table of Isotopes*, Vol. II (John Wiley, 1996).
[48] P.J. Twin et al., Phys. Rev. Lett. 57 (1986) 811.